

1 **Influence of enhanced Asian NO_x emissions on ozone in the Upper Troposphere and**
2 **Lower Stratosphere (UTLS) in chemistry climate model simulations**

3 Chaitri R.¹, Suvarna Fadnavis^{1*}, Rolf Müller², Ayantika D. C.¹, Felix Ploeger², Alexandru Rap³

4 ¹Indian Institute of Tropical Meteorology, Pune, India

5 ²Forschungszentrum Jülich GmbH, IEK7, Jülich, Germany

6 ³School of Earth and Environment, University of Leeds, Leeds, United Kingdom

7 *Email of corresponding author: suvarna@tropmet.res.in

8

9 **Abstract:**

10 **The Asian summer monsoon (ASM) anticyclone is the most pronounced circulation pattern in the**
11 **Upper Troposphere and Lower Stratosphere (UTLS) during the Northern Hemisphere summer.** Asian
12 summer monsoon convection plays an important role in efficient vertical transport from the surface to
13 the upper-level anticyclone. In this paper we investigate the potential impact of enhanced
14 anthropogenic nitrogen oxides (NO_x) on the distribution of ozone in the UTLS using the fully-coupled
15 aerosol chemistry climate model, ECHAM5-HAMMOZ. Ozone in the UTLS is influenced both by the
16 convective uplift of ozone precursors and by the uplift of enhanced NO_x induced tropospheric ozone
17 anomalies. We performed anthropogenic NO_x emission sensitivity experiments over India and China.
18 **In these simulations, covering the years 2000-2010 anthropogenic NO_x emissions have been increased**
19 **by 38% over India and by 73% over China with respect to the emission base year 2000. These emission**
20 **increases are comparable to the observed linear trends of 3.8 % per year over India and 7.3% per year**
21 **over China during the period 2000 to 2010. Enhanced** NO_x emissions over India by 38 % and China by
22 73 % increase the ozone radiative forcing in the ASM Anticyclone (15°-40°N, 60°-120°E) by 16.3 mW
23 m⁻² and 78.5 mW m⁻² respectively. These elevated NO_x emissions **produce** significant warming over the
24 Tibetan Plateau and increase precipitation over India due to a strengthening of the monsoon Hadley

25 circulation.

26 However increase in NO_x emissions over India by 73% (similar to the observed increase over China),
27 results in large amount of ozone production over the Indo Gangetic plain and Tibetan Plateau. The
28 higher ozone concentrations, in turn, induce a reversed monsoon Hadley circulation and negative
29 precipitation anomalies over India. The associated subsidence suppresses vertical transport of NO_x and
30 ozone into the ASM anticyclone.

31 Key words: Asian summer monsoon, Tropospheric ozone, Tropospheric NO_x, NO_x transport, Upper
32 troposphere and lower stratosphere, Ozone radiative forcing.

33

34 1. Introduction

35 Rapid economic development and urbanization in Asia has resulted in an unprecedented growth in
36 anthropogenic emissions of nitrogen oxides (NO_x), carbon monoxide (CO), carbon dioxide (CO₂),
37 methane (CH₄). Many of these species affect concentrations of tropospheric ozone, which is both an
38 important polluting agent and a greenhouse gas (Wild and Akimoto, 2001; Chatani et al 2014; Revell et
39 al., 2015). Ground based and satellite observations show a large amount of these ozone precursors
40 concentrated over India and China (Sinha et al., 2014; Richter et al., 2005; Jacob et al., 1999; Zhao et
41 al., 2013; Gu et al., 2014). Studies show that tropospheric ozone production over Asia is controlled by
42 the abundance of NO_x and VOCs (Sillman, 1995, Lei et al., 2004, Zhang et al., 2004 and Tie et al.,
43 2007), with large regions such as India and China being NO_x limited regions. Therefore, increased NO_x
44 in these regions leads to an increase in ozone concentrations (Yamaji et al., 2006; Sinha et al., 2014;
45 Fadnavis et al., 2014). Recently, positive trends in Asian tropospheric column NO₂ have been reported,
46 i.e. 3.8 % yr⁻¹ over India, using SCanning Imaging Absorption SpectroMeter for Atmospheric
47 CHartography (SCIAMACHY) observations for the period 2003-2011 (Ghude et al., 2013), and 7.3%
48 yr⁻¹ over China using Ozone Monitoring Instrument (OMI) observations for the period 2002-2011

49 (Schneider and van der A., 2012). Lightning contributes to the production of NO_x in the middle and
50 upper troposphere (Barret et al, 2016). Over the Asian region, lightning contributes ~40% to NO_x and
51 20% to ozone production in the middle and upper troposphere during the monsoon season (Tie et al.
52 2001; Fadnavis et al. 2015). The upper tropospheric ozone concentration is determined by in-situ
53 production from both lightning and ozone precursors which are transported from the boundary layer
54 (Sóvde et al., 2011; Barret et al, 2016).

55 Tropospheric ozone has a warming effect on climate, its estimated radiative forcing due to
56 increased concentrations since pre-industrial times being 0.4 W m⁻², with a 5 to 95% confidence range
57 of (0.2 to 0.6 W m⁻²) (Stevenson et al., 2013; Myhre et al., 2013). Previous studies highlighted the
58 importance of the tropical tropopause region for ozone radiative forcing (Lacis et al, 1990; Riese et al.,
59 2012; Rap et al., 2015) and showed that ozone perturbations exert a large influence on the thermal
60 structure of the atmosphere (e.g., Thuburn and Craig, 2002; Foster and Shine 1997). A recent study
61 based on Atmospheric Chemistry and Climate Model Intercomparison Project (ACCMIP) models
62 reported that NO_x and CH₄ are the greatest contributors in determining tropospheric ozone radiative
63 forcing (Stevenson et al., 2013).

64 Asian Summer Monsoon (ASM) convection efficiently transports Asian pollutants from the
65 boundary layer into the Upper Troposphere and Lower Stratosphere (UTLS) (Randel and Park, 2006;
66 Randel et al. 2010; Fadnavis et al., 2013, 2015). Studies pertaining to modeling and trajectory analysis
67 confirm this finding (Li et al., 2005; Park et al., 2007; Randel et al., 2010; Chen et al., 2012; Vogel et
68 al., 2015, 2016). Satellite observations show the confinement of a number of chemical constituents like
69 water vapor (H₂O), CO, CH₄, ethane, hydrogen cyanide (HCN), PAN and aerosols, within the ASM
70 anticyclone (Park et al., 2004, 2007, 2008; Li et al., 2005; Randel and Park, 2006; Xiong et al., 2009;
71 Randel et al. 2010; Lawrence et al., 2011; Abad et al., 2011; Fadnavis et al., 2013;2014;2015; Barret et
72 al., 2016) which has potential implications on stratospheric chemistry and dynamics. Thus the rise in

73 anthropogenic emissions over the ASM region alters the chemical composition of the UTLS (Lawrence
74 et al., 2011; Fadnavis et al., 2014, 2015) during the monsoon season. Another prominent feature of the
75 satellite observations is an ozone minimum in the ASM anticyclone (near 100 hPa) (Gettelman et al.,
76 2004; Konopka et al., 2010; Braesicke et al., 2011). This ozone minimum is linked to upward transport
77 of ozone poor air masses (Gettelman et al., 2004; Park et al., 2007; Kunze et al., 2010). Observations
78 show that convectively lifted air masses arriving in the anticyclone are ozone poor but rich in ozone
79 precursors. Balloon sonde observations show that ozone variations near the anticyclone are strongly
80 correlated with temperature near the tropopause (Tobo et al., 2008). Thus the linkage of low ozone and
81 high concentrations of ozone precursors with the temperature variation in the anticyclone is an open
82 question.

83 In this study we ask the question ‘how do increasing Asian NO_x emissions and the associated
84 ozone production affect ozone radiative forcing and monsoon circulation?’. We perform sensitivity
85 experiments of increased anthropogenic NO_x emissions using the state-of-the-art ECHAM5-HAMMOZ
86 (European Centre General Circulation Model version5) chemistry climate model (Roeckner et al.,
87 2003; Horowitz et al., 2003; Stier et al., 2005). We estimate the ozone radiative forcing for the different
88 anthropogenic NO_x emission scenarios, together with associated changes in temperature and the
89 monsoon circulation. The paper is organized as follows: in Section 2 the data and model set up are
90 described; the results are summarized in Section 3 and discussed in Section 4, followed by conclusions
91 given in Section 5.

92

93 **2. Data description and Model setup**

94 **2.1 Satellite measurements**

95 Earth Observing System (EOS) microwave limb sounder (MLS) is one of the four instruments
96 on the NASA’s EOS Aura satellite flying in the polar sun-synchronous orbit. It measures the thermal

97 emissions at millimeter and sub millimeter wavelengths (Waters et al., 2006). It performs 240 limb
98 scans per orbit with a footprint of ~6 km across-track and ~200 km along-track, providing ~3500
99 profiles per day. MLS also measures vertical profiles of temperature, ozone, CO, H₂O, and many other
100 constituents in the mesosphere, stratosphere and upper troposphere (Waters et al., 2006). In the UTLS,
101 MLS has a vertical resolution of about 3 km. MLS vertical profiles of ozone show good agreements
102 with the Stratospheric Aerosol and Gas Experiment II (SAGE-II), Halogen Occultation Experiment
103 (HALOE), Atmospheric Chemistry Experiment (ACE) and ozonesonde measurements (Froidevaux et
104 al.,2006). The MLS ozone profiles are considered to be useful in the range of 215 – 0.46 hPa (Livesey
105 et al., 2005). In this study we analyze the MLS level 2 (version 4) ozone mixing ratios data for the
106 period 2004 – 2013. The data has been interpolated to potential temperature levels and gridded
107 horizontally, within latitude bins of equal area (with the equatorial bin of 150km width) and longitude
108 bins of about 8.5 degrees. This data can be accessed from <http://mls.jpl.nasa.gov/>. For comparison,
109 simulated ozone is convolved with the MLS averaging kernel (Livesey et al. 2011).

110

111 **2.2 Model simulation and experimental setup**

112 We employ the aerosol-chemistry-climate model ECHAM5-HAMMOZ which comprises the
113 general circulation model ECHAM5 (Roeckner et al., 2003), the tropospheric chemistry module,
114 MOZART2 (Horowitz et al 2003) and the aerosol module, Hamburg aerosol model (HAM) (Stier et al.,
115 2005). It includes NO_x, VOC and aerosol chemistry. The gas phase chemistry is based on the chemical
116 scheme provided by the MOZART-2 model (Horowitz et al., 2003) which includes detailed chemistry
117 of the O_x-NO_x hydrocarbon system with 63 tracers and 168 reactions. The O(¹D) quenching reaction
118 rates used are taken from Sander et al., (2003) and isoprene nitrates chemistry taken from Fiore et al.,
119 (2005). The dry deposition in ECHAM5-HAMMOZ follows the scheme given by Ganzeveld and
120 Lelieveld (1995). Soluble trace gases like HNO₃ and SO₂ are also subject to wet deposition. In-cloud

121 and below-cloud scavenging follows the scheme given by Stier et al. (2005). **Interactive calculation of**
122 **cloud droplet number concentration is according to Lohmann et al (1999) and ice crystal number**
123 **concentrations are according to Kärcher and Lohmann (2002). The convection scheme is based on the**
124 **mass flux scheme developed by Tiedke (1989).**

125
126 The model is run at a T42 spectral resolution corresponding to about $2.8^\circ \times 2.8^\circ$ in the horizontal
127 dimension and 31 vertical hybrid $\sigma - p$ levels from the surface to 10 hPa. **In our model simulations,**
128 **emissions from anthropogenic sources and biomass burning are from the year 2000 RETRO project**
129 **data set (available at <http://eccad.sedoo.fr/>) (Schultz et al., 2004; 2005; 2007; 2008). Emissions of SO₂,**
130 **BC and OC are based on the AEROCOM-II emission inventory, also for the year 2000 (Dentener et al.,**
131 **2006). The distribution of NO_x emission mass flux ($\text{kg m}^{-2} \text{s}^{-1}$) averaged for the Asian summer**
132 **monsoon season (June–September) is shown in Supplementary Fig. S1. It shows high values over the**
133 **Indo Gangetic Plains and East China.** Other details of model parameterizations, emissions and
134 **evaluation** are described by Fadnavis et al. (2013; 2014; 2015) and Pozzoli et al. (2008a, b; 2011). Each
135 of our model experiments consists of continuous simulations for eleven years from 2000 to 2010. **The**
136 **base year for emissions is taken as 2000 and emissions were repeated every year throughout the**
137 **simulation period.** Meteorology varied due to **varying monthly** mean sea surface temperature (SST) and
138 sea ice concentration (SIC). The AMIP2 SSTs and SIC **varying for** the period 2000 – 2010 were
139 specified as a lower boundary condition.

140 In order to understand the impact of enhanced **anthropogenic** NO_x emissions on the distribution
141 of ozone in the UTLS, **sensitivity** simulations were performed for the period 2000 – 2010. The
142 experimental set up is the same as described by Fadnavis et al., (2015). The four **simulations** analyzed
143 in this study are: (1) a reference experiment (CTRL) and three sensitivity experiments (referred to as
144 experiments 2 - 4), where the **anthropogenic** NO_x emissions over India and China are scaled in
145 accordance with the observed trends. In experiment (2), **anthropogenic** NO_x emissions are increased

146 over India by 38% (Ind38), in experiment (3) increases-over China by 73% (Chin73) are prescribed. In
147 order to analyze the effects of similar NO_x percentage increases over India and China, NO_x emissions
148 are increased over India by 73% (Ind73) in experiment (4). The emission perturbations were obtained
149 from observed NO₂ trends of 3.8% per year over India (Ghude et al., 2013) and 7.3% per year over
150 China (Schneider and van der A., 2012). Hiboll et al. (2013) also reported similar increasing NO_x
151 values over megacities in India and China. All four simulations use the same VOC and CO emissions
152 and they all include NO_x production due to lightning (lightning-on) and soil emissions (see Table 1,
153 showing details pertaining to these experiments). Therefore NO_x or ozone anomalies obtained from
154 difference between Ind38, Ind73 and Chin73 with respective to CTRL simulation do not have an
155 impact of lightning or soil emissions as they are same in all the simulations.

156 In addition, a series of four lightning-off simulations were performed for the same period and
157 boundary conditions as experiments 1-4 (these simulations are the same as the ones documented by
158 Fadnavis et al. (2015))The impact of lightning on NO_x production is estimated by comparing the CTRL
159 (lightning-on) simulation with lightning-off simulations.

160 The accuracy of the simulation of the monsoon circulation will likely depend on the model
161 resolution and increased vertical resolution may improve the model performance (Druyan et al., 2008;
162 Abhik et al., 2014). While we acknowledge the limitations of our relatively course vertical resolution
163 (dictated by our computational resources), the model is still capable of reasonably simulating the
164 general regional spatial pattern of precipitation and low-level circulation (Rajeevan et al., 2005) (see
165 Supplementary Fig. S2, showing simulated seasonal mean precipitation and circulation at 850 hPa in
166 the CTRL simulation).

167 The heating rates and radiative forcings associated with the ozone changes in our three
168 sensitivity simulations are calculated using the Edwards and Slingo (1996) radiative transfer model and
169 the fixed dynamical heating approximation for stratospheric temperature adjustment. Similarly to

170 previous studies (Riese et al., 2012; Bekki et al., 2013; Rap et al., 2015), we used the off-line version of
171 the model, with six shortwave and nine longwave bands, and a delta-Eddington 2-stream scattering
172 solver at all wavelengths.

173

174 **3. Results**

175 **3.1 Comparison with MLS satellite measurements in the UTLS**

176 The spatial distributions of ozone mixing ratios from MLS observations at 100 hPa and from
177 the CTRL ECHAM5-HAMMOZ simulation at 90 hPa (the nearest model level) after smoothing with
178 the averaging kernel of MLS are illustrated in Fig. 1a and Fig. 1b, respectively. The climatological
179 horizontal winds plotted in the figure clearly show the anticyclonic upper level monsoon circulation.
180 Recent attempts to characterize the extent of the anticyclone are based either on potential vorticity on
181 isentropic surfaces or geopotential height on pressure surfaces. Here we apply both characterizations of
182 the anticyclone and show the PV contour related to the maximum PV gradient on 380K (calculated
183 from ERA-Interim reanalysis following Ploeger et al., 2015), and the 270m geopotential height
184 anomaly as proposed by Barret et al. (2016). The close agreement of both methods shows that from a
185 climatological point of view the two criteria yield a very similar picture of the anticyclonic circulation
186 and the related trace gas confinement. Locally and at particular dates, however, differences may be
187 larger with potential vorticity correlating better with confined trace gas anomalies than geopotential
188 height (e.g., Garny and Randel, 2013; Ploeger et al., 2015). The spatial pattern of low ozone
189 concentrations in the monsoon anticyclone is well simulated in the model. It is in good agreement with
190 MLS (90-140 ppbv), MIPAS (80-120 ppbv) and SAGE II (<150ppbv) measurements (Kunze et al.,
191 2010; Randel et al., 2001; Randel and Park 2006; Park et al., 2007).

192 Vertical profiles of ozonesonde measurements (averaged for the monsoon season during 2001-
193 2009) at Indian stations, Delhi (28.61°N, 77.23°E), Pune (18.52°N, 73.85°E) and Thiruvananthapuram

194 (8.48°N, 76.95E) are compared with MLS measurements and ECHAM5-HAMMOZ simulated ozone
195 mixing ratios in Figs. 1(c)-(e). ECHAM5-HAMMOZ simulations show good agreement with MLS data
196 between 200 hPa and 50 hPa at all three stations. Comparison of ozonesonde observations with the
197 ECHAM5-HAMMOZ simulation shows reasonably good agreement at Pune, compared to Delhi and
198 Thiruvananthapuram where there are some discrepancies. The simulated ozone mixing ratios are lower
199 than ozonesonde measurements by 10-40 ppb between 500 – 90 hPa at Pune and by ~70-90 ppb in the
200 upper troposphere (500-150 hPa) at Delhi. At Thiruvananthapuram, while at altitudes below 375 hPa,
201 simulated ozone mixing ratios show good agreement with ozonesonde data, at the altitudes above 375
202 hPa, simulated values are lower than observations by ~20-70 ppb. The differences between model and
203 ozonesonde data may be due to different grid sizes: the ECHAM5-HAMMOZ model grid size is ~280
204 km, while balloon observations are within ~30-180 km spatial range (balloon typically drifts ~30–180
205 km horizontally). In addition, previous work comparing these model simulations with various aircraft
206 observations during the monsoon season, found a reasonable agreement for PAN, NO_x, HNO₃ and O₃
207 mixing ratios (Fadnavis et al., 2015).

208

209 **3.2 Transport of enhanced NO_x emissions into the UTLS**

210 Recent satellite observations and model simulations quantified the impact of convective
211 transport of boundary layer pollution into the ASM anticyclone during the Asian summer monsoon
212 season (Gettelman et al., 2004; Randel et al., 2010; Fadnavis et al., 2013, 2014, 2015). These pollutants
213 are further transported across the tropopause as evident in satellite observations of, e.g. water vapour
214 (Bian, 2012), hydrogen cyanide (HCN) (Randel, 2010), CO (Schoeberl et al., 2006), Peroxyacetyl
215 nitrate (PAN) (Fadnavis et al., 2014; 2015), aerosols (Vernier et al., 2015, Fadnavis et al., 2013). To
216 understand the influence of monsoon convection on the vertical distribution of NO_x we show zonal and
217 meridional cross sections over India and China. Vertical distributions of NO_x averaged for the monsoon

218 season over Indian latitudes (8°N-35°N), and Chinese latitudes (20°N-45°N) as obtained from CTRL
219 simulations are shown in the Supplementary Figs. S3(a) and S3(b) respectively. These figures show
220 elevated levels of NO_x extending from the surface to the upper troposphere over India and China. The
221 wind vectors along with the distribution of cloud droplet number concentration (CDNC) and ice crystal
222 number concentration (ICNC), (Supplementary Figs. S4(a), S4(b) and S4(c)) indicate strong convective
223 transport from the Bay of Bengal (BOB), South China Sea and southern slopes of Himalayas which
224 might lift the boundary layer NO_x to the upper troposphere.

225 During the monsoon season, the NO_x distribution in the UTLS is also influenced by lightning,
226 in addition to transport from anthropogenic sources. Lightning activity during this season was found to
227 be more pronounced in Asia, compared to the other monsoon regions such as North America, South
228 America and Africa (Ranalkar and Chaudhari, 2009; Penki and Kamra, 2013). In our simulations, we
229 find that lightning produces 40-70% of NO_x over north India and Bay of Bengal and 40-60% over the
230 Tibetan Plateau and West China region (Supplementary Fig. S5).

231 Fig. 2 shows the vertical distribution of anthropogenic NO_x anomalies obtained from the Ind38,
232 Ind73, Chin73 simulations, compared with the CTRL simulation. Ind38 and Chin73 simulations show
233 that the convective winds over the Bay of Bengal (80-90°E) (Figs. 2(a) and 2(c)) and at the southern
234 flank_of the Himalayas (Figs. 2(d) and 2(f)) lift up the enhanced NO_x emissions to the upper
235 troposphere (UT). While most transport is mainly into the UT, parts of it also occur into the lower
236 stratosphere, with cross tropopause transport being particularly evident in the Chin73 simulation (Figs.
237 2(c) and 2(f)). Randel and Park (2006) and Randel et al. (2010) also reported that pollution transported
238 by Asian monsoon convection enters the stratosphere. Our results are also in good agreement with
239 previous studies indicating significant vertical transport due to strong monsoon convection from the
240 southern slopes of Himalayas (Fu et al., 2006, Fadnavis et al., 2013; 2014) and the South China Sea
241 (Park et al 2009; Chen et al., 2012). In the upper troposphere, NO_x is transported over Iran and Saudi

242 Arabia along the descending branch of the **large scale monsoon** circulation (Rodwell and Hoskins,
243 1995). However, the cross tropopause transport is not present in the Ind73 simulation, where it is
244 inhibited by the wind anomalies that show a descending branch over central India ($\sim 20^\circ\text{N}$, 75°E) (Figs.
245 2(b) and 2(e)). These descending wind anomalies may also be related to the associated ozone radiative
246 forcing and temperature changes, as discussed in Section 4.

247

248 **3.3 Impact of enhanced anthropogenic NO_x on the tropospheric ozone distribution**

249 We **calculate** the change in ozone production over India and China due to enhanced NO_x
250 emissions in the Ind38, Ind73 and Chin73 simulations with respect to the CTRL **simulation**. Figure 3,
251 showing longitude-pressure cross sections of net ozone production (ppt/day) changes, indicates that the
252 majority of this additional ozone production occurs in the lower troposphere. At altitudes below 300
253 hPa, the ozone production and loss vary between -15 ppt day^{-1} and 15 ppt day^{-1} . In the upper
254 troposphere (300-150 hPa), the estimated amount of **additional** net ozone production in Ind38 and
255 Ind73 simulation is $3\text{-}7 \text{ ppt day}^{-1}$, while in the Chin73 simulation it is $\sim 3\text{-}13 \text{ ppt day}^{-1}$. We also simulate
256 ozone loss near the tropopause in the Ind73 simulation (Figure 3b). We note that these ozone anomalies
257 are not driven by lightning NO_x , as this is included in all simulations. **It is interesting to understand**
258 **ozone production over the highly populated Indo Gangetic Plain and Tibetan Plateau region. A**
259 **longitude pressure cross section over this region show that ozone production over the Indo Gangetic**
260 **Plain and Tibetan Plateau in Ind73 is (20-25ppt/day) is much larger than Ind38 (6-20 ppt/day) in the**
261 **lower troposphere (Supplementary Fig. S6).**

262 **Figure 4** shows the vertical distribution of ozone anomalies induced by enhanced anthropogenic
263 NO_x emissions in the three perturbation experiments compared to the CTRL simulation, averaged over
264 India and China. Although the air mass in the monsoon anticyclone is relatively poor in ozone
265 (**Fig.1(b)**), the elevated amounts of ozone anomalies in response to enhanced anthropogenic NO_x

266 emissions are clearly seen in Fig. 4. This may be partially due to convective transport of enhanced-
267 NO_x-emission induced ozone anomalies produced in the lower troposphere, and partially due to
268 chemical ozone production from convectively transported boundary layer ozone precursors. Ozone
269 anomalies are enhanced near 300-200 hPa over west Asia (40-60°E) (Figs. 4a-c), possibly due to the
270 vertical convective transport of ozone anomalies and precursors and also from subsequent horizontal
271 transport in the monsoon anticyclone (Barret et al., 2016).

272 Latitude-pressure cross sections of enhanced-NO_x-emission induced ozone anomalies plotted in
273 Figs. 4(d) and 4(f) illustrate how convection over the Bay of Bengal, the southern slopes of the
274 Himalayas and the South China Sea lifts the enhanced ozone anomalies from India and China into the
275 upper troposphere. These ozone anomalies are also transported further across the tropopause and into
276 the lower stratosphere, where ozone production is also driven by photolysis and NO_x anomalies.

277 In the Ind73 simulation, similarly to the NO_x anomaly distribution (Figs. 2(b) and 2(e)), the
278 descending branch of circulation over central India also suppresses the vertical transport of ozone
279 anomalies across the tropopause (Figs. 4(b) and 4(e)). This subsidence may be related to ozone heating
280 rate changes, as there is significant increase in ozone production over the Indo Gangetic plain and
281 Tibetan Plateau in the lower troposphere due to enhanced anthropogenic NO_x emissions (Section 4).

282

283 **3.4 Distribution of NO_x and ozone in the anticyclone**

284 The distributions of NO_x and ozone anomalies in the monsoon anticyclone region in the Ind38,
285 Ind73 and Chin73 simulations with respect to the CTRL simulation are shown in Figs. 5(a)-(f). A
286 maximum in the NO_x anomalies in the ASM anticyclone (60°E to 120°E) is seen in all the simulations.
287 NO_x anomalies are high at the eastern part of the monsoon anticyclone since convective injection into
288 the anticyclone occurs mainly in that region (Fadnavis et al., 2013). Increase in NO_x anomalies in the
289 Ind38 simulation is higher (Fig. 5(a)) than that in the Ind73 simulation (Figs. 5(b)), mainly due to

290 descending motion over central India in the Ind73 simulation, as seen in the previous sections. In
291 contrast to NO_x anomalies, ozone anomalies in Ind38 are lower than Ind73, especially in the north-
292 eastern part of anticyclone. Satellite observations also show high ozone precursors and low ozone
293 amounts in the anticyclone (Park et al., 2007; Barret et al., 2016). Similarly, the Chin73 simulation
294 shows higher values of NO_x anomalies (>18%) and strong negative ozone anomalies (~-8%) in the
295 north eastern region of the monsoon anticyclone (Figs. 5(c) and 5(f)). Figure 5 also shows that the
296 tropical easterly jet transports NO_x and ozone (from India and China) to Saudi Arabia, Iran and Iraq.

297

298 4. Discussion

299 To estimate the radiative impact of the simulated ozone changes, we use the offline version of
300 the Edwards and Slingo (1996) radiative transfer model. Figure 6 shows the radiative forcing caused by
301 the ozone changes in each of the three sensitivity simulations compared to the CTRL simulation. The
302 overall increase in tropospheric ozone (see Figure 4) has a warming effect on climate, with the regional
303 average radiative forcing in the monsoon anticyclone (15°N-40°N, 60-120°E) estimated at 16.3 mW m⁻²,
304 69.9 mW m⁻², and 78.5 mW m⁻² in the Ind38, Ind73, and Chin73 simulations, respectively.

305 We also investigate the impact on the atmospheric heating rates caused by the ozone changes.
306 Figure 7 shows the zonal mean heating rate anomalies for the Ind38, Ind73 and Chin73 simulations,
307 compared to the CTRL simulation. These three simulations show positive and negative heating rates
308 anomalies between 400-200 hPa. However, in the upper troposphere and lower stratosphere (200-50
309 hPa) ozone heating rates are negative over Indo Gangetic plain (20-30°N) and Tibetan Plateau (30-
310 40°N) region. In Ind73 simulation, ozone heating rate anomalies are positive in the lower troposphere
311 over the Indo Gangetic plain (1000-750 hPa) and Tibetan plateau (600-400 hPa). This may be due to
312 large amount of ozone production in the lower troposphere over these regions (Fig. S6). This heating
313 may produce changes in the circulation leading to ascending motion over the Tibetan Plateau and a

314 descending branch over central India ($\sim 20^\circ\text{N}$), i.e. a reversal of monsoon Hadley circulation (Fig. 9(b)).

315 Figures 8 shows latitude pressure cross-section of temperature anomalies (K) obtained from
316 Ind38, Ind73 and Chin73 simulations. Ind38 and Chin73 simulations show anomalous warming in the
317 upper troposphere over the Tibetan Plateau while it is subdued in the Ind73 simulation. Upper
318 tropospheric warming over the Tibetan plateau is one of the key factors responsible for the ASM
319 circulation (Flohn 1957; Yanai et al., 1992; Meehl, 1994; Li and Yanai, 1996; Wu and Zhang, 1998).
320 Flohn (1957, 1960) suggested that upper tropospheric warming over the Tibetan plateau leads to
321 increased Indian summer monsoon rainfall by enhancing the cross-equatorial circulation that brings
322 rainfall to India (Rajagopalan and Molnar, 2013, Vinoj et al., 2014). Goswami et al., (1999) also
323 reported that there is a strong correlation between Hadley circulation and monsoon precipitation.

324 Figures 9(a)-(c) depict the change in monsoon Hadley cell circulation (averaged over 70°E -
325 100°E) obtained from the difference in the Ind38, Ind73 and Chin73 and CTRL simulations. The Ind38
326 and Chin 73 simulations show a strengthening of the Hadley circulation; a strong ascending branch of
327 the Hadley cell around 10° - 20°N (Fig. 9(a)), whereas the tilted descending branch of Hadley cell is seen
328 over 20°N in the Ind73 simulation (Fig. 9(b)). In Ind73 simulation ozone heating rates are positive and
329 negative in the vertical direction near $\sim 20^\circ\text{N}$ (Fig 7 (b)) which might have attributed tilted descending
330 branch of Hadley cell. Consequently, precipitation anomalies over the Indian region (70° - 90°E ; 8° - 35°
331 N) are positive (0.3 to 0.9 mm day^{-1}) in the Ind38 and Chin73 simulations (Figs. 9(d) and 9(f)), whereas
332 they are negative in the Ind73 simulation (-0.3 to -0.6 mm day^{-1}) (Fig. 9(e)). In the upper troposphere
333 (250 hPa - 100 hPa), Ind73 simulation shows subsidence while Chin73 simulation shows ascending
334 motion at these levels over the Indian region. Upper tropospheric subsidence in Ind73 simulation might
335 have contributed to the weak positive and negative precipitation anomalies over the North Indian
336 region (Fig. 9(e)). The Chin73 simulation shows subsidence near 22°N below 200 hPa and ascending
337 motion above it. The Chin73 simulation shows ascending motion near 12°N rising up to 110 hPa , which

338 leads to positive precipitation anomalies over the Indian peninsula.

339 Thus, enhanced Indian (Ind38) and Chinese (Chin73) NO_x emissions increase warming over the
340 Tibetan plateau and enhance precipitation over India via a strengthening of the monsoon Hadley
341 circulation. Remarkably, a further increase of NO_x emissions over India (Ind73) leads to high amounts
342 of ozone in the lower troposphere over the Indo Gangetic plain and Tibetan Plateau. The related ozone
343 heating induces a reversal of the monsoon Hadley circulation, thereby resulting in negative
344 precipitation anomalies.

345 5. Conclusions

346 In this paper we investigate the potential impacts of enhanced anthropogenic NO_x emissions on
347 ozone production and distribution during the monsoon season using the state-of-the-art ECHAM5-
348 HAMMOZ model simulations. We performed sensitivity experiments for anthropogenic NO_x
349 enhancements of 38% over India (Ind38 simulation) and 73% over China (Chin73 simulation) in
350 accordance with recently observed trends of 3.8% per year over India and 7.3% per year over China
351 (Ghude et al., 2013; Schneider and van der A., 2012). In another experiment, anthropogenic NO_x
352 emissions over India are increased by 73%, equal to Chinese emissions (Ind73 simulation).

353 These simulations show that an increase in anthropogenic NO_x emissions (over India and
354 China) increases ozone production in the lower and mid-troposphere. The monsoon convection at the
355 southern flank of the Himalayas (80-90°E) and over the Bay of Bengal lifts up the NO_x and ozone
356 anomalies from India across the tropopause into the lower stratosphere. Cross tropopause transport also
357 occurs over China due to convection over the South China Sea.

358 Increase in NO_x emissions in the Ind38, Ind73 and Chin73 simulations leads to increase in
359 ozone radiative forcings, in the anticyclone (15°N-40°N, 60°E-120°E) of 16.25 mWm⁻², 69.88 mW m⁻²,
360 and 78.51 mW m⁻² in the Ind38, Ind73, and Chin73 simulations, respectively. Enhanced ozone

361 production (Ind38 and Chin73 simulations) increases ozone heating rates which cause anomalous
362 warming over the **Tibetan plateau**. Further increase in NO_x emissions over the India region (Ind73
363 simulation) produces anomalous heating in the lower troposphere over the Indo Gangetic Plain and
364 Tibetan Plateau. **This warming elicits the reversal of the monsoon Hadley cell circulation. The**
365 **descending branch of the monsoon Hadley circulation over the central India impedes vertical transport**
366 **of ozone and NO_x anomalies.**

367 In the Ind38 and Chin73 simulations, anomalous warming over the **Tibetan plateau** results in a
368 strengthening of the monsoon Hadley circulation over India and elicits positive precipitation (0.3 to 0.9
369 mm day⁻¹) anomalies over India. However, in Ind73 simulations the reversal of the Hadley circulation
370 and the concurrent subdued warming in the upper troposphere over the **Tibetan plateau** results in
371 negative precipitation anomalies (-0.3 to -0.6 mm day⁻¹) over India.

372

373 *Acknowledgement:* Dr. S. Fadnavis and C. Roy acknowledges with gratitude Dr. Krishnan, Director of
374 IITM, for his encouragement during the course of this study. We also thank **two** anonymous reviewers
375 for their valuable suggestions for improvement of this manuscript. Authors acknowledge the High
376 Power Computing Centre (HPC) in IITM, Pune, India, for providing computer resources. **Part of the**
377 **research leading to these results has received funding from the European Community's Seventh**
378 **Framework Programme (FP7/2007-2013) in the frame of the StratoClim project under grant agreement**
379 **number 603557. Felix Ploeger was supported by the Helmholtz Young Investigators Group grant A-**
380 **SPECi (VH-NG-1128).**

381

382 **References:**

- 383 Abad G. G., Allen N. D. C., Bernath P. F., Boone C. D., McLeod S. D., Manney G. L., Toon G. C.,
384 Carouge C., Wang Y., Wu S., Barkley M. P., Palmer P. I., Xiao Y., and Fu T. M.: Ethane, ethyne
385 and carbon monoxide concentrations in the upper troposphere and lower stratosphere from ACE
386 and GEOS-Chem: a comparison study, *Atmos. Chem. Phys.*, 11, 9927–9941, 2011.
387 doi:10.5194/acp-11-9927-2011, 2011.
- 388 Abhik S., Mukhopadhyay P., Goswami B. N., Evaluation of mean and intraseasonal variability of
389 Indian summer monsoon simulation in ECHAM5: identification of possible source of bias,
390 *Climate Dynamics*, Volume 43, Issue 1, pp 389–406, 2014.
- 391 Barret, B., Sauvage, B., Bennouna, Y., and Le Flochmoen, E.: Upper-tropospheric CO and O₃ budget
392 during the Asian summer monsoon, *Atmos. Chem. Phys.*, 16, 9129-9147, doi:10.5194/acp-16-
393 9129-2016, 2016.
- 394 Bekki, S., Rap, A., Poulain, V., Dhomse, S., Marchand, M., Lefevre, F., Forster, P. M., Szopa, S. and
395 Chipperfield, M. P.: Climate impact of stratospheric ozone recovery, *Geophys. Res. Lett.*,
396 40(11),2796-2800,doi:10.1002/grl.50358,2013.
- 397 Bian, J., Pan, L. L., Paulik, L., Vömel, H., Chen, H., and Lu, D.: In situ water vapor and ozone
398 measurements in Lhasa and Kunming during the Asian summer monsoon, *Geophys. Res.*
399 *Lett.*, 39, L19808, doi:10.1029/2012GL052996, 2012.
- 400 Braesicke, P., Smith, O. J., Telford, P., & Pyle, J. A.: Ozone concentration changes in the Asian
401 summer monsoon anticyclone and lower stratospheric water vapour: An idealised model study.
402 *Geophysical Research Letters*, 38(3), doi: 10.1029/2010GL046228, 2011.
- 403 Chatani, S., Amann, M., Goel, A., Hao, J., Klimont, Z., Kumar, A., Mishra, A., Sharma, S., Wang, S.
404 X., Wang, Y. X., and Zhao, B.: Photochemical roles of rapid economic growth and potential
405 abatement strategies on tropospheric ozone over South and East Asia in 2030, *Atmos. Chem.*
406 *Phys.*, 14, 9259-9277, doi:10.5194/acp-14-9259-2014, 2014.
- 407 Chen, B., Xu, X., D, Yang, S., and Zhao, T. L.: Climatological perspectives of air transport from
408 atmospheric boundary layer to tropopause layer over Asian monsoon regions during boreal
409 summer inferred from Lagrangian approach, *Atmos. Chem. Phys.*, 12, 5827–5839,
410 doi:10.5194/acp-12-5827-2012. 2012.
- 411 Dentener F., Kinne S., Bond T., Boucher O., Cofala J., Generoso S., Ginoux P., Gong S., Hoelzemann
412 J. J., Ito A., Marelli L., Penner J. E., Putaud J.-P., Textor C., Schulz M., Werf G. R. van der, and
413 Wilson J.: Emissions of primary aerosol and precursor gases in the years 2000 and 1750
414 prescribed data-sets for AeroCom, *Atmos. Chem. Phys.*, 6, 4321-4344, doi:10.5194/acp-6-
415 4321-2006, 2006.
- 416 Druyan L. M., Fulakeza M. and Lonergan P.: The impact of vertical resolution on regional model
417 simulation of the west African summer monsoon, *Int. J. Climatol.* 28: 1293–1314, DOI:
418 10.1002/joc.1636, 2008.
- 419 Edwards, J. M., and Slingo, A.: Studies with a flexible new radiation code .1. Choosing a
420 configuration for a large-scale model, *Quart. Jour. Roy. Met. Soc.*, 122(531), 689-719,
421 doi:10.1002/qj.49712253107,1996.
- 422 Fadnavis, S., Semeniuk, K., Pozzoli, L., Schultz, M. G., Ghude, S. D., Das, S., and Kakatkar, R.:
423 Transport of aerosols into the UTLS and their impact on the Asian monsoon region as seen in a
424 global model simulation, *Atmos. Chem. Phys.*, 13, 8771–8786, doi:10.5194/acp-13-8771-2013,
425 2013.
- 426 Fadnavis, S., Semeniuk, K., Schultz, M. G., Kiefer, M., Mahajan, A., Pozzoli, L., and Sonbawane, S.:
427 Transport pathways of peroxyacetyl nitrate in the upper troposphere and lower stratosphere
428 from different monsoon systems during the summer monsoon season. *Atmos. Chem. and*

429 Phys., 15, doi:10.5194/acp-15-11477-2015, 11477-11499, 2015.

430 Fadnavis, S., Semeniuk, K., Schultz, M. G., Mahajan, A., Pozzoli, L., Sonbawane, S., and Kiefer, M.:
431 Transport pathways of peroxyacetyl nitrate in the upper troposphere and lower stratosphere
432 from different monsoon systems during the summer monsoon season, *Atmos. Chem. Phys.*
433 *Discuss.*, 14, 20159–20195, doi:10.5194/acpd-14-20159-2014, 2014.

434 Fiore, A. M., Horowitz, L. W., Purves, D. W., Levy II, H., Evans, M. J., Wang, Y., Li, Q., and
435 Yantosca, R. M.: Evaluating the contribution of changes in isoprene emissions to surface ozone
436 trends over the eastern United States, *J. Geophys. Res.*, 110, D12303,
437 doi:10.1029/2004JD005485, 2005.

438 Flohn, H.: Large-scale aspects of the summer monsoon in South and East Asia, *J. Meteor. Soc. Japan*,
439 75, 180–186, doi: 551.553.21:551.589.5, 1957.

440 Flohn, H.: Recent investigations on the mechanism of the “Summer Monsoon” of Southern and
441 Eastern Asia, *Proc. Symp. Monsoon of the World*, 1960.

442 Forster, F., Piers, M., and Keith, P. Shine: Radiative forcing and temperature trends from stratospheric
443 ozone changes, *J. Geophys Res*, 102, 10841-10855, 1997.

444 Froidevaux, L., Livesey, N. J., Read, W. G., Jiang, Y. B., Jimenez, C. J., Filipiak, M. J., Schwartz, M.
445 J., Santee, M. L., Pumphrey, H. C., Jiang, J. H., Wu, D. L., Manney, G. L., Drouin, B. J.,
446 Waters, J. W., Fetzer, E. J., Bernath, P. F., Boone, C. D., Walker, K. A., Jucks, K. W., Toon, G.
447 C., Margitan, J. J., Sen, B., Webster, C. R., Christensen, L. E., Elkins, J. W., Atlas, E., Ueb, R.
448 A., and Hendershot, R.: Early validation analyses of atmospheric profiles from EOS MLS on
449 the Aura satellite. *IEEE Trans. Geosci. Remote Sensing* 44, 1106 – 1121, doi:
450 10.1109/TGRS.2006.864366, 2006.

451 Fu, R., Hu, Y. L., Wright, J. S., Jiang, J. H., Dickinson, R.E., Chen, M. X., Filipiak, M., Read, W. G.,
452 Waters, J. W., and Wu, D. L.: Short circuit of water vapor and polluted air to the global
453 stratosphere by convective transport over the Tibetan Plateau, *P. Natl. Acad. Sci. USA*, 103,
454 5664–5669, doi:10.1073/pnas.0601584103, 2006.

455 Ganzeveld, L. and Lelieveld, J.: Dry deposition parameterization in a chemistry general circulation
456 model and its influence on the distribution of reactive trace gases, *J. Geophys. Res.*, 100,
457 20999–21012, doi:10.1029/95JD02266, 1995.

458 Garny, H. and Randel, W. J.: Dynamic variability of the Asian monsoon anticyclone observed in
459 potential vorticity and correlations with tracer distributions, *J. Geophys. Res. Atmos.*, 118,
460 13,421–13,433, doi:10.1002/2013JD020908, 2013.

463 Gettelman, A., Kinnison, D. E., Dunkerton, T. J., and Brasseur, G. P.: Impact of monsoon circulations
464 on the upper troposphere and lower stratosphere, *J. Geophys. Res.*, 109, D22101,
465 doi:10.1029/2004jd004878, 2004.

466 Ghude, S. D., Kulkarni, S. H., Jena, C., Pfister, G. G., Beig, G., Fadnavis, S., and van der A R. J.:
467 Application of satellite observations for identifying regions of dominant sources of nitrogen
468 oxides over the Indian Subcontinent, *J. Geophys. Res.*, 118, 1–15, doi:10.1029/2012JD017811,
469 2013.

470 Goswami, B. N., Krishnamurthy, V., and Annamalai, H.: A broad-scale circulation index for the
471 interannual variability of the Indian summer monsoon. *Q. J. R. Meteorol. soc.*, 125, 611-633,
472 doi: 10.1002/qj.49712555412, 1999.

473 Gu, D., Wang, Y., Smeltzer, C., and Boersma, K. F.: Anthropogenic emissions of NO_x over China:
474 Reconciling the difference of inverse modeling results using GOME-2 and OMI
475 measurements, *J. Geophys. Res. Atmos.*, 119, doi:10.1002/ 2014JD021644, 2014.

478 Hilboll, A., Richter, A., and Burrows, J. P.: Long-term changes of tropospheric NO₂ over megacities
479 derived from multiple satellite instruments, *Atmos. Chem. Phys.*, 13, 4145–4169,
480 doi:10.5194/acp-13-4145-2013, 2013.

481 Horowitz, L. W., Walters, S., Mauzerall, D. L., Emmons, L. K., Rasch, P. J., Granier, C., Tie, X.,
482 Lamarque, J., Schultz, M. G., Tyndall, G. S., Orlando, J. J., and Brasseur, G. P.: A global
483 simulation of tropospheric ozone and related tracers, Description and evaluation of MOZART,
484 version 2, *J. Geophys. Res.*, 108, 4784, doi:10.1029/2002JD002853, 2003.

485 Jacob, D. J., Logan, J. A., and Murti, P. P.: Effect of rising Asian emissions on surface ozone in the
486 United States, *Geophys. Res. Lett.*, 26, 2175–2178, doi:10.1029/1999GL900450, 1999.

487 Kärcher B. and U. Lohmann, A parameterization of cirrus cloud formation: Homogeneous freezing of
488 supercooled aerosols, *J. Geophys. Res.* 107, NO. D2, 4010, 10.1029/2001JD000470, 2002.

489 Konopka, P., Groöß, J.U., Günther, G., Ploeger, F., Pommrich, R., Müller, R. and Livesey, N.: Annual
490 cycle of ozone at and above the tropical tropopause: observations versus simulations with the
491 Chemical Lagrangian Model of the Stratosphere (CLaMS), *Atmos. Chem. Phys.*, 10(1), 121-
492 132, doi: www.atmos-chem-phys.net/10/121/2010/, 2010.

493 Kunze, M., Braesicke, P., Langematz, U., Stiller, G., Bekki, S., Brühl, C., Chipperfield, M., Dameris,
494 M., Garcia, R. and Giorgetta, M.: Influences of the Indian summer monsoon on water vapor
495 and ozone concentrations in the UTLS as simulated by chemistry-climate models, *J. Clim.*,
496 23(13), 3525-3544, doi: http://dx.doi.org/10.1175/2010JCLI3280.1, 2010.

498 Lacis Andrew, A., Donald Wuebbles, J., and Jennifer Logan A., Radiative Forcing of climate by
499 Changes in the Vertical Distribution of Ozone, *J. Geophys. Res.*, 95 , 9971-9981, doi:
500 10.1029/JD095iD07p09971, 1990.

501 Lawrence, M. G.: Atmospheric science: Asia under a high-level brown cloud, *Nat. Geosci.*, 4, 352–
502 353, doi:10.1038/ngeo1166, 2011.

503 Lei, W., Zhang, R., Tie, X., and Hess, P.: Chemical characterization of ozone formation in the
504 Houston-Galveston area. *J. Geophys. Res.*, 109, doi: 10.1029/2003JD004219, 2004.

505 Li, C. and Yanai M.: The onset and interannual variability of the Asian summer monsoon in relation to
506 land–sea thermal contrast, *J. Clim.* 9: 358–375, doi: http://dx.doi.org/10.1175/1520-
507 0442(1996)009<0358:TOAIVO>2.0.CO;2, 1996.

508 Li, Q., Jiang, J. H., Wu, D. L., Read, W. G., Livesey, N. J., Waters, J. W., Zhang, Y., Wang, B.,
509 Filipiak, M. J., Davis, C. P., Turquety, S., Wu, S., Park, R. J., Yantosca, R. M., and Jacob, D. J.:
510 Convective outflow of south Asian pollution: a global CTM simulation compared with EOS
511 MLS observations, *Geophys. Res. Lett.*, 32, doi: http://dx.doi.org/10.1029/2005GL022762,
512 doi: 10.1029/2005GL022762, 2005.

513 Livesey, N. J., Read, W. G., Filipiak, M. J., Froidevaux, L., Harwood, R. S., Jiang, J. H., Jimenez, C.,
514 Pickett, H. M., Pumphrey, H. C., Santee, M. L., Schwartz, M. J., Waters, J. W., and Wu, D. L.:
515 EOS MLS Version 1.5 Level 2 data quality and description document, JPL, California, 2005.

516 Livesey, N. J., Read, W. G., Froidevaux, L., Lambert, A., Manney, G. L., Pumphrey, H. C., Santee, M.
517 L., Schwartz, M. J., Wang, S., Cofield, R. E., Cuddy, D. T., Fuller, R. A., Jarnot, R. F., Jiang, J.
518 H., Knosp, B. W., Stek, P. C., Wagner, P. A., and Wu, D. L.: Version 3.3 Level 2 data quality
519 and description document. Tech Rep. JPL D-33509, Jet Propulsion Laboratory, available at:
520 http://mls.jpl.nasa.gov (last access: 17 August 2015), 2011.

521 Lohmann, U., J. Feichter, C. C. Chuang, and J. E. Penner, Predicting the number of cloud droplets in
522 the ECHAM GCM, *J. Geophys. Res.*, 104, 9169 – 9198, 1999.

523 Meehl, G. A.: Coupled land-ocean-atmosphere processes and South Asian monsoon variability,
524 *Science*, 266, 263–267, doi: 10.1126/science.266.5183.263, 1994.

525 Myhre, G., et al., Anthropogenic and natural radiative forcing, in *Climate Change 2013: The Physical
526 Science Basis. Contribution of Working Group I to the Fifth Assessment Report of the
527 Intergovernmental Panel on Climate Change*, edited by T. F. Stocker et al., pp. 659–740,
528 Cambridge Univ. Press, Cambridge, U. K., and New York, 2013.

533 Park, M., Randel, W. J., Emmons, L. K., Bernath, P. F., Walker, K. A., and Boone, C. D.: Chemical

534 isolation in the Asian monsoon anticyclone observed in Atmospheric Chemistry Experiment
535 (ACE-FTS) data, *Atmos. Chem. Phys.*, 8, 3, 757-764, doi: [www.atmos-chem-](http://www.atmos-chem-phys.net/8/757/2008/)
536 [phys.net/8/757/2008/](http://www.atmos-chem-phys.net/8/757/2008/), 2008.

537 Park, M., Randel, W. J., Emmons, L. K., and Livesey, N. J.: Transport pathways of carbon monoxide in
538 the Asian summer monsoon diagnosed from Model of Ozone and Related Tracers (MOZART),
539 *J. Geophys. Res.*, 114, D08303, doi:10.1029/2008jd010621, 2009.

540 Park, M., Randel, W. J., Gettelman, A., Massie, S. T., and Jiang, J.H.: Transport above the Asian
541 summer monsoon anticyclone inferred from Aura Microwave Limb Sounder tracers, *J.*
542 *Geophys. Res.*, 112, D16309, doi:10.1029/2006jd008294, 2007.

543 Park, M., Randel, W. J., Kinnison, D. E., Garcia, R. R., and Choi, W.: Seasonal variation of methane, water vapour, and
544 nitrogen oxides near the tropopause: Satellite observations and model simulations, *J. Geophys. Res.*, 109,
545 D03302, doi:10.1029/2003JD003706, 2004.

546 Penki, R. K. and Kamra, A. K.: Lightning distribution with respect to the monsoon trough position
547 during the Indian summer monsoon season, *J. Geophys. Res.*, 118, 4780–4787,
548 doi:10.1002/jgrd.50382, 2013.

549 Ploeger, F., Gottschling, C., Griessbach, S., Groß, J.-U., Guenther, G., Konopka, P., Müller, R., Riese,
550 M., Stroh, F., Tao, M., Ungermann, J., Vogel, B., and von Hobe, M.: A potential vorticity-based
551 determination of the transport barrier in the Asian summer monsoon anticyclone, *Atmos.*
552 *Chem. Phys.*, 15, 13145-13159, doi:10.5194/acp-15-13145-2015, 2015.

553 Pozzoli, L., Bey, I., Rast, J. S., Schultz, M. G., Stier, P., and Feichter, J.: Trace gas and aerosol
554 interactions in the fully coupled model of aerosol-chemistry-climate ECHAM5- HAMMOZ: 1.
555 Model description and insights from the spring 2001 TRACE-P experiment, *J. Geophys. Res.*,
556 113, D07308, doi:10.1029/2007JD009007, 2008a.

557 Pozzoli, L., Bey, I., Rast, J. S., Schultz, M. G., Stier, P., and Feichter, J.: Trace gas and aerosol
558 interactions in the fully coupled model of aerosol-chemistry-climate ECHAM5- HAMMOZ: 2.
559 Impact of heterogeneous chemistry on the global aerosol distributions, *J. Geophys. Res.*, 113,
560 D07309, doi:10.1029/2007JD009008, 2008b.

561 Pozzoli, L., Janssens-Maenhout, G., Diehl, T., Bey, I., Schultz, M. G., Feichter, J., Vignati, E., and
562 Dentener, F.: Re-analysis of tropospheric sulfate aerosol and ozone for the period 1980–2005
563 using the aerosol-chemistry-climate model ECHAM5-HAMMOZ, *Atmos. Chem. Phys.*, 11,
564 9563–9594, doi:10.5194/acp-11-9563-2011, 2011.

565 Rajeevan M., Bhatte J., Kale J.D and Lal B.: Development of High Resolution Daily Gridded Rainfall
566 Data for the Indian Region, *Met. Monograph Climatology No. 22/2005*, National Climate
567 Centre India Meteorological Department. Pune 411 005, India, 2005.

568 Rajagopalan, B., and Molnar, P.: Signatures of Tibetan Plateau heating on Indian summer monsoon
569 rainfall variability, *J. Geophys. Res. Atmos.*, 118, 1170–1178, doi:10.1002/jgrd.50124, 2013.

570 Ranalkar, M. R. and Chaudhari, H. S.: Seasonal variation of lightning activity over the Indian
571 subcontinent, *Meteorol. Atmos. Phys.*, 104, 125–134, doi: 10.1007/s00703-009-0026-7, 2009.

572 Randel, W. J., and Park M.: Deep convective influence on the Asian summer monsoon anticyclone and
573 associated tracer variability observed with Atmospheric Infrared Sounder (AIRS), *J. Geophys.*
574 *Res.*, 111, D12314, doi:10.1029/2005JD006490, 2006.

575 Randel, W. J., Park, M., Emmons, L., Kinnison, D., Bernath, P., Kaley Walker, A., Boone, C., and
576 Pumphrey, H.: Asian Monsoon Transport of Pollution to the Stratosphere *Science*, 328(5978),
577 611-613, doi: 10.1126/science.1182274, 2010.

578 Randel, W. J., Wu, F., Gettelman, A., Russell, J. M., Jawodny, J. M., and Oltmans, S. J.: Seasonal
579 variation of water vapor in the lower stratosphere observed in Halogen Occultation Experiment
580 data, *J. Geophys. Res.*, 106, 14,313 – 14,325, doi: 10.1029/2001JD000485, 2001.

581 Rap, A., Richards, N., A., D., Forster, P., M., Monks, S., Arnold, S., R., Chipperfield, M.: Satellite

582 constraint on the tropospheric ozone radiative effect, *Geophys. Res. Lett.*, 42, [5074-5081](https://doi.org/10.1002/2015GL064037).doi:10.1002/2015GL064037, 2015.

583

584 Revell, L. E., Tummon, F., Stenke, A., Sukhodolov, T., Coulon, A., Rozanov, E., Garny, H., Grewe, V.,
585 and Peter, T.: Drivers of the tropospheric ozone budget throughout the 21st century under the
586 medium-high climate scenario RCP 6.0, *Atmos. Chem. Phys.*, 15, 5887-5902, doi:10.5194/acp-
587 15-5887-2015, 2015.

588 Richter, A., John Burrows, P., Hendrik, N., Granier C., and Niemeier, U.: Increase in tropospheric
589 nitrogen dioxide over China observed from space; 437, doi:10.1038/nature04092, 2005.

590 Riese, M., Ploeger, F., Rap, A., Vogel, B., Konopka, P., Dameris, M. and Forster, P.: Impact of
591 uncertainties in atmospheric mixing on simulated UTLS composition and related radiative
592 effects, *J. Geophys. Res.: Atmos.*, 117(D16), doi: 10.1029/2012JD017751, 2012.

593 Rodwell, M. J. and Hoskins, B. J.: Monsoons and the dynamics of deserts, *QJRMS*, 122(534), 1385-
594 1404, doi: 10.1002/qj.49712253408, 1995.

595 Roeckner, E., Bauml, G., Bonaventura, L., Brokopf, R., Esch, M., Giorgetta, M., Hagemann, S.,
596 Kirchner, I., Kornbluh, L., Manzini, E., Rhodin, A., Schlese, U., Schulzweida, U., and
597 Tompkins, A.: The atmospheric general circulation model ECHAM5: Part 1, Tech. Rep. 349,
598 Max Planck Institute for Meteorology, Hamburg, 2003.

599 Sander, S. P., Fried, R. R., Barker, J. R., Golden, D. M., Kurylo, M. J., Wine, P. H., J. Abbatt, P. D., 25
600 Burkholder, J. B., Kolb, C. E., Moortgat, G. K., Huie, R. E., and Orkin, V. L.: Chemical
601 kinetics and photochemical data for use in atmospheric studies, evaluation number 14, JPL
602 Publ. 02-25, Jet Propul. Lab., Calif. Inst. Of Technol., Pasadena, available at:
603 http://jpldataeval.jpl.nasa.gov/pdf/JPL_02-25_rev02.pdf, 2003.

604 Schneider, P. and van der A. R. J.: A global single-sensor analysis of 2002–2011 tropospheric nitrogen
605 dioxide trends observed from space, *J. Geophys. Res.*, 117, D16309,
606 doi:10.1029/2012JD017571, 2012.

607 Schoeberl, M. R., Duncan, B. N., Douglass, A. R., Waters, J., Livesey, N., Read, W., and Filipiak, M.:
608 The carbon monoxide tape recorder. *Geophys. Res. Lett.*, 33(12), doi:
609 10.1029/2006GL026178, 2006.

610 Schultz, M. G., Heil, A., Hoelzemann, J. J., Spessa, A., Thonicke, K., Goldammer, J. G., Held, A. C.,
611 Pereira, J. M. C., and van het Bolscher, M.: Global wildland fire emissions from 1960 to 2000,
612 *Global Biogeochem. Cy.*, 22, GB2002, doi:10.1029/2007GB003031, 2008.

613 Schultz, M., Backman, L., Balkanski, Y., Bjoerndalsaeter, S., Brand, R., Burrows, J., Dalsoeren, S., de
614 Vasconcelos, M., Grodtmann, B., Hauglustaine, D., Heil, A., Hoelzemann, J., Isaksen, I.,
615 Kaurola, J., Knorr, W., Ladstaetter-Weienmayer, A., Mota, B., Oom, D., Pacyna, J., Panasiuk,
616 D., Pereira, J., Pulles, T., Pyle, J., Rast, S., Richter, A., Savage, N., Schnadt, C., Schulz, M.,
617 Spessa, A., Staehelin, J., Sundet, J., Szopa, S., Thonicke, K., van het Bolscher, M., van Noije,
618 T., van Velthoven, P., Vik, A. and Wittrock, F.: REanalysis of the TROospheric chemical
619 composition over the past 40 years (RETRO). A long-term global modeling study of
620 tropospheric chemistry. Final Report, Tech. rep., Max Planck Institute for Meteorology,
621 Hamburg, Germany, 2007.

622 Schultz, M.G., Heil A., Hoelzemann, J. J., Spessa, A., Thonicke, K., Goldammer, J., Held, A.C,
623 Pereira, J. M., Van Het Bolscher, M.: Global Wildland Fire Emissions from 1960 to 2000,
624 doi:10.1029/2007GB003031 , *Global Biogeochemical Cycles* 22 (GB2002) : 17 PP, 2005

625 Sillman, S.: The use of NO_y, H₂O₂, and HNO₃ as indicators for ozone-NO_x-hydrocarbon sensitivity in
626 urban locations. *J. Geophys. Res.*, 100, 14,175–14,188, doi: 10.1029/94JD02953, 1995.

627 Sinha, V., Kumar, V., and Sarkar, C.: Chemical composition of pre-monsoon air in the Indo-Gangetic
628 Plain measured using a new air quality facility and PTR-MS: high surface ozone and strong
629 influence of biomass burning, *Atmos. Chem. Phys.*, 14, 5921–5941, 2014. doi:10.5194/acp-14-

630 5921-2014, 2014.

631 Søvde, O. A., Hoyle, C. R., Myhre, G., and Isaksen, I. S. A.: The HNO₃ forming branch of the HO₂ +
632 NO reaction: pre-industrial-to-present trends in atmospheric species and radiative forcings,
633 *Atmos. Chem. Phys.*, 11, 8929–8943, 2011; doi:10.5194/acp-11-8929-2011, 2011.

634 Stevenson, D. S., P. J. Young, Vaishali, N., Lamarque, J. F., Drew, T., Shindell, Voulgarakis, A., and
635 Skeie R. B.: Tropospheric ozone changes, radiative forcing and attribution to emissions in the
636 Atmospheric Chemistry and Climate Model Intercomparison Project (ACCMIP), *Atmos.*
637 *Chem. Phys.*, 13, 3063-3085, doi:10.5194/acp-13-3063-2013, 2013.

638 Stier, P., Feichter, J., Kinne, S., Kloster, S., Vignati, E., Wilson, J., Ganzeveld, L., Tegen, I., Werner,
639 M., Balkanski, Y., Schulz, M., Boucher, O., Minikin, A., and Petzold, A.: The aerosol-climate
640 model ECHAM5-HAM, *Atmos. Chem. Phys.*, 5, 1125–1156, doi:10.5194/acp-5-1125-2005,
641 2005.

642 Thuburn, J. and Craig, G.C.: On the temperature structure of the tropical stratosphere, *Journal of*
643 *Geophysical Research: Atmospheres*, 107(D2), doi: 10.1029/2001JD000448, 2002.

644 Tie, X. X., Zhang, R., Brasseur, G., Emmons, L., and Lei, W.: Effects of lightning on reactive nitrogen
645 and nitrogen reservoir species in the troposphere, *J. Geophys. Res.-Atmos.*, 106, 3167– 3178,
646 doi:10.1029/2000JD900565, 2001.

647 Tie, X., Madronich, S., Li, G.H., Ying, Z.M., Zhang, R., Garcia, A., Lee-Taylor, and J., Y. Liu.
648 Characterizations of chemical oxidants in Mexico City: a regional chemical/dynamical model
649 (WRF-Chem) study, *Atmos. Environ.*, 41, 1989–2008, doi:10.1016/j.atmosenv.2006.10.053,
650 2007.

651 **Tiedtke, M.: A comprehensive mass flux scheme for cumulus parameterization in large-scale models,**
652 ***Mon. Weather Rev.*, 117(8), 1779–1800, 1989.**

653 Tobo, Y., Iwasaka, Y., Zhang, D., Shi, G., Kim, Y. S., Tamura, K., and Ohashi, T.: Summertime
654 “ozone valley” over the Tibetan Plateau derived from ozonesondes and EP/TOMS data,
655 *Geophys. Res. Lett.*, 35, L16801, doi:10.1029/2008GL03434, 2008.

656 Vernier, J.-P., T. D. Fairlie, M. Natarajan, F. G. Wienhold, J. Bian, B. G. Martinsson, S. Crumeyrolle,
657 L. W. Thomason, and Bedka, K.: Increase in upper tropospheric and lower stratospheric
658 aerosol levels and its potential connection with Asian Pollution, *J. Geophys. Res. Atmos.*, 120,
659 1608–1619, doi:10.1002/2014JD022372, 2015.

660 Vinoj, V., Rasch, P.J., Wang, H., Yoon, J.H., Ma, P.L., Landu, K. and Singh, B.: Short-term modulation
661 of Indian summer monsoon rainfall by West Asian dust, *Nature Geoscience*, 7(4), 308-313,
662 doi:10.1038/ngeo2107, 2014.

663 Vogel B., Günther G., Müller R., Groöß, and Riese M.: Impact of different Asian source regions on the
664 composition of the Asian J.-u. monsoon anticyclone and of the extratropical lowermost
665 stratosphere, *Atmos. Chem. Phys.*, 15, 13699–13716, doi:10.5194/acp-15-13699-2015, 2015.

666 **Vogel, B., Günther, G., Müller, R., Groöß, J.-U., Afchine, A., Bozem, H., Hoor, P., Krämer, M., Müller,**
667 **S., Riese, M., Rolf, C., Spelten, N., Stiller, G. P., Ungermann, J., and Zahn, A.: Long-range**
668 **transport pathways of tropospheric source gases originating in Asia into the northern lower**
669 **stratosphere during the Asian monsoon season 2012, *Atmos. Chem. Phys. Discuss.*,**
670 **doi:10.5194/acp-2016-463, revised paper accepted for ACPD, 2016.**

671 Waters, J. W., Froidevaux, L., Harwood, R.S., Jarnot, R.F., Pickett, H. M., Read, W. G., Siegel, P. H.,
672 Cofield, R. E., Filipiak, M. J., Flower, D. A., Holden, J. R., Lau, G. K., Livesey, N. J., Manney,
673 G. L., Pumphrey, H. C., Santee, M. L., Wu, D. L., Cuddy, D. T., Lay, R. R., Loo, M. S., Perun,
674 V. S., Schwartz, M. J., Stek, P. C., Thurstans, R. P., Boyles, M. A., Chandra, S., Chavez, M. C.,
675 Chen, G. S., Chudasama, B. V., Dodge, R., Fuller, R. A., Girard, M.A., Jiang, J. H., Jiang, Y.,
676 Knosp, B. W., LaBelle, R. C., Lee, K. A., Miller, D., Oswald, J. E., Patel, N. C., Pukala, D.
677 M., Quintero, O., Scaff, D. M., Snyder, W. V., Tope, M. C., Wagner, P. A., and Walch, M. J.:

679 The Earth Observing System Microwave LimbSounder (EOS MLS) on the Aura satellite.
680 IEEE Trans, Geosci., Remote Sensing, 44, 1075 – 1092, doi: 10.1109/TGRS.2006.873771,
681 2006.

682 Wild, O., and Akimoto, H.: Intercontinental transport of ozone and its precursors in a three-
683 dimensional global CTM, *J. Geophys. Res.*, 106(D21), 27729-27744, doi:
684 <http://dx.doi.org/10.1029/2000JD000123>, 2001.

685 Wu, G. X., and Zhang, Y. S.: Tibetan Plateau forcing and the timing of the monsoon onset over South
686 Asia and the South China Sea, *Mon Wea Rev* 126:913–927, doi:
687 [http://dx.doi.org/10.1175/1520-0493\(1998\)126<0913:TPFATT>2.0.CO;2](http://dx.doi.org/10.1175/1520-0493(1998)126<0913:TPFATT>2.0.CO;2), 1998.

688 Xiong, X., Houweling S., Wei J., Maddy E., Sun F., and Barnet C.: Methane plume over south Asia
689 during the monsoon season: satellite observation and model simulation, *Atmos. Chem. Phys.*,
690 9, 783–794, doi:10.5194/acp-9-783-2009, 2009.

691 Yamaji, K., T. Ohara, I. Uno, H. Tanimoto, J. Kurokawa, and Akimoto H.: Analysis of the seasonal
692 variation of ozone in the boundary layer in East Asia using the Community Multiscale Air
693 Quality model: what controls surface ozone levels over Japan?, *Atmos. Environ.*, 40, 1856–
694 1868, 2006.

695 Yanai, M., Li, C., Song, Z.: Seasonal heating of the Tibetan Plateau and its effects on the evolution of
696 the Asian summer monsoon, *J Meteor Soc Japan*, 70, 189–221, 1992.

697 Zhang, R.W., Lei, X., and Hess, T. P.: Industrial emissions cause extreme diurnal urban ozone
698 variability. *Proc. Natl. Acad. Sci.*, 101, 6346–6350, doi: 10.1073/pnas.0401484101, 2004.

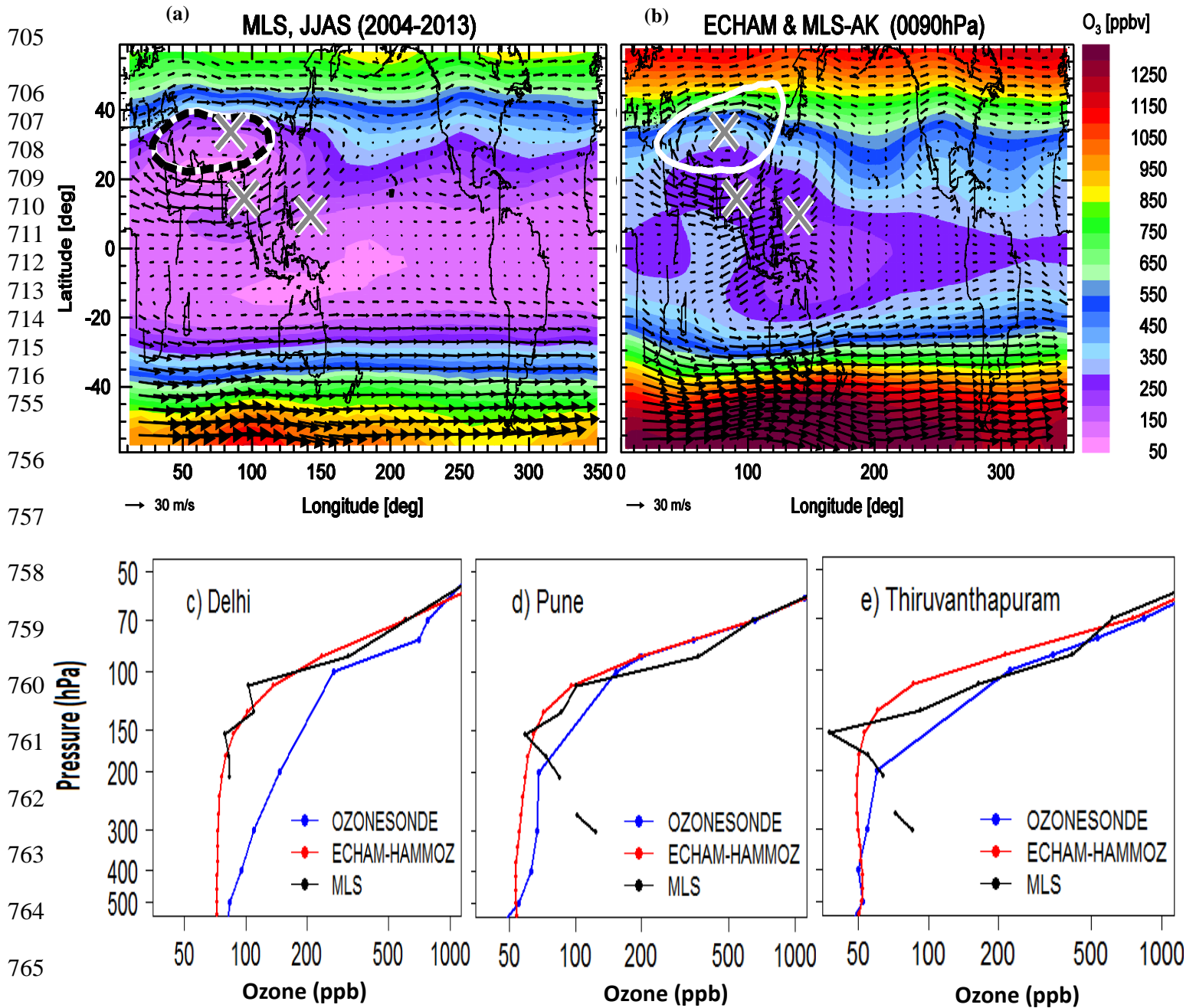
699 Zhao, B., Wang, S. X., Liu, H., Xu, J. Y., Fu, K., Klimont, Z., Hao, J. M., He, K. B., Cofala, J., and
700 Amann, M.: NO_x emissions in China: historical trends and future perspectives, *Atmos. Chem.*
701 *Phys.*, 13, 9869–9897, doi:10.5194/acp-13-9869-2013, 2013.

702

703

Table 1: Details of the sensitivity experiments (2000 - 2010).

Name of experiment	Prescribed SSTs	Emissions 704
CTRL	AMIP2 SST and SIC varying from 2000 – 2010	RETRO anthropogenic NO _x emissions for the year 2000.
Ind38	AMIP2 SST and SIC varying from 2000 – 2010	RETRO anthropogenic NO _x emissions for the year 2000 are increased by 38% over India for 11 years period 2000-2010
Chin73	AMIP2 SST and SIC varying from 2000 – 2010	RETRO anthropogenic NO _x emissions for the year 2000 are increased by 73% over China for 10 years period 2000-2010.
Ind73	AMIP2 SST and SIC varying from 2000 – 2010	RETRO anthropogenic NO _x emissions for the year 2000 are increased by 73% over India for 10 years period 2000-2010.



767 Figure 1: Distribution of ozone mixing ratio (ppb) during the monsoon season (June-September)
 768 obtained from (a) MLS observations at 100 hPa, and (b) from ECHAM-HAMMOZ at 90hPa. Black
 769 arrows indicate wind vectors, the black dashed contour shows the PV-gradient based transport barrier
 770 of the anticyclone (calculated following Ploeger et al., 2015), and the white contour shows the 270m
 771 geopotential height anomaly, corresponding to the anticyclone edge definition by Barret et al. (2016)
 772 (Meteorological data shows climatological July fields from ERA-Interim reanalysis (a) ERA-Interim

773 reanalysis and (b) ECHAM5-HAMMOZ. The ECHAM5-HAMMOZ ozone distribution is smoothed
774 using the MLS averaging kernel. Grey crosses highlight the regions of the Tibetan plateau, Bay of
775 Bengal and South China Sea. Bottom panels show the vertical distribution of seasonal (June-
776 September) mean ozone mixing ratios (ppb) from ozonesonde (2001-2009), MLS (2004-2013) and
777 ECHAM5-HAMMOZ CTRL simulation at the (c) Delhi, (d) Pune, and (e) Thiruvananthpuram Indian
778 stations.
779

780

781

782

783

784

785

786

787

788

789

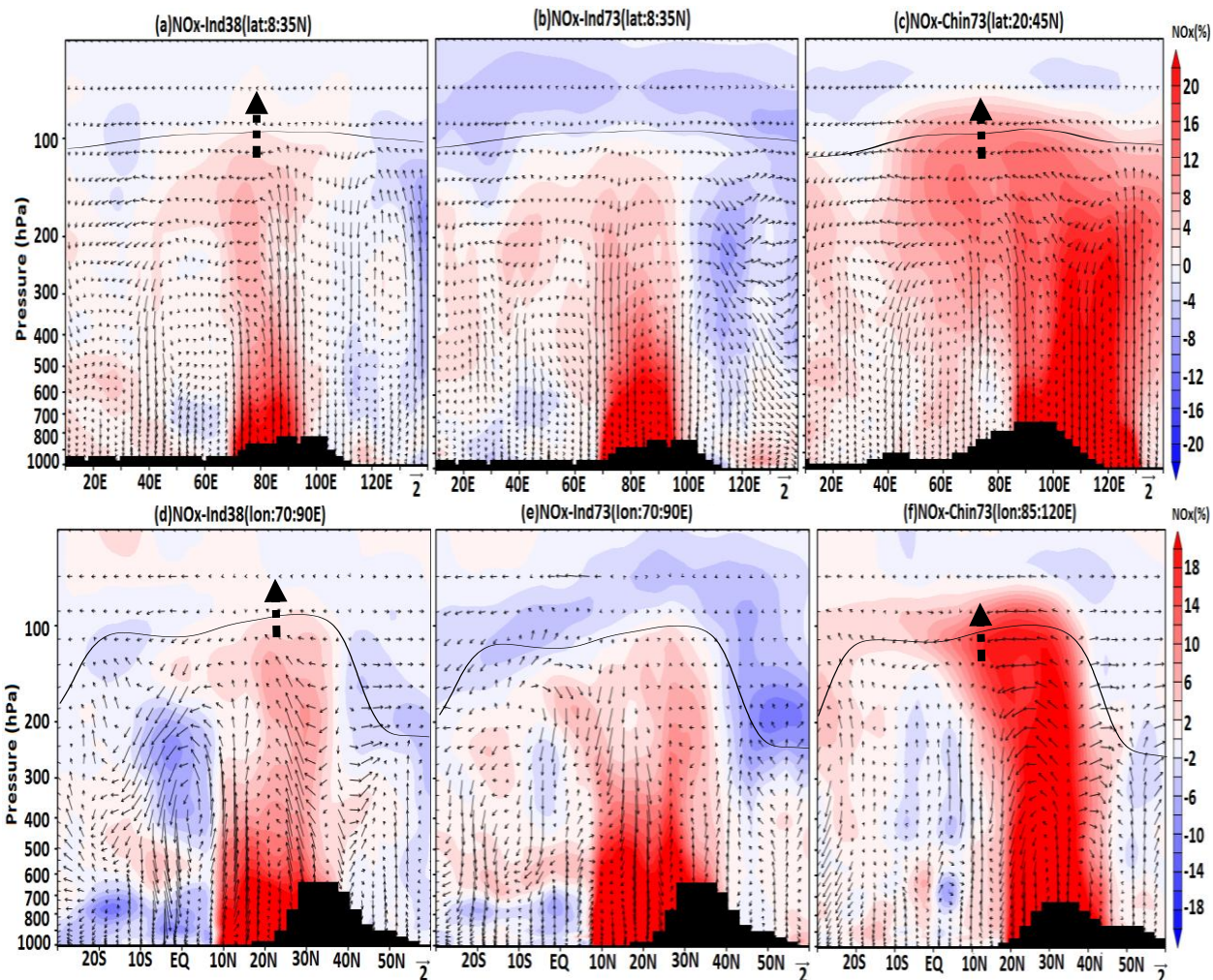
790

791

792

793

794



795 Figure 2: Longitude pressure cross-sections of percentage NO_x anomalies averaged for the monsoon
796 season (June-September) obtained from (a) Ind38 (averaged over 8°N - 35°N), (b) Ind73 (averaged over
797 8°N - 35°N), and (c) Chin73 (averaged over 20°N - 45°N) simulations. Latitude pressure cross-sections of
798 percentage NO_x anomalies averaged for the monsoon season (June-September) obtained from (d)
799 Ind38 (averaged over 70°E - 90°E), (e) Ind73 (averaged over 70°E - 90°E), and (f) Chin73 (averaged over
800 85°E - 120°E) simulations. Black arrows indicate wind vectors (the vertical velocity field has been
801 scaled by 300), the black line represents the tropopause, and the black dashed arrows indicate the cross
802 tropopause transport.

803

804

805

806

807

808

809

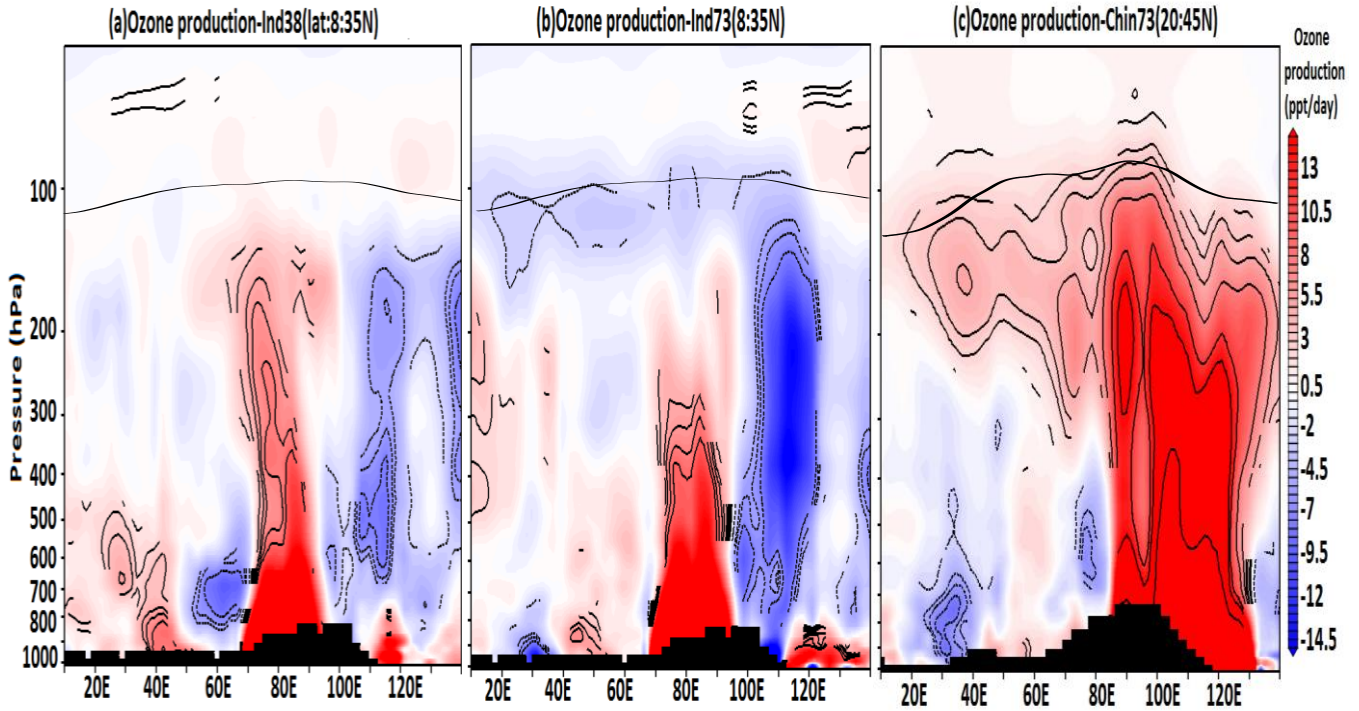
810

811

812

813

814



815

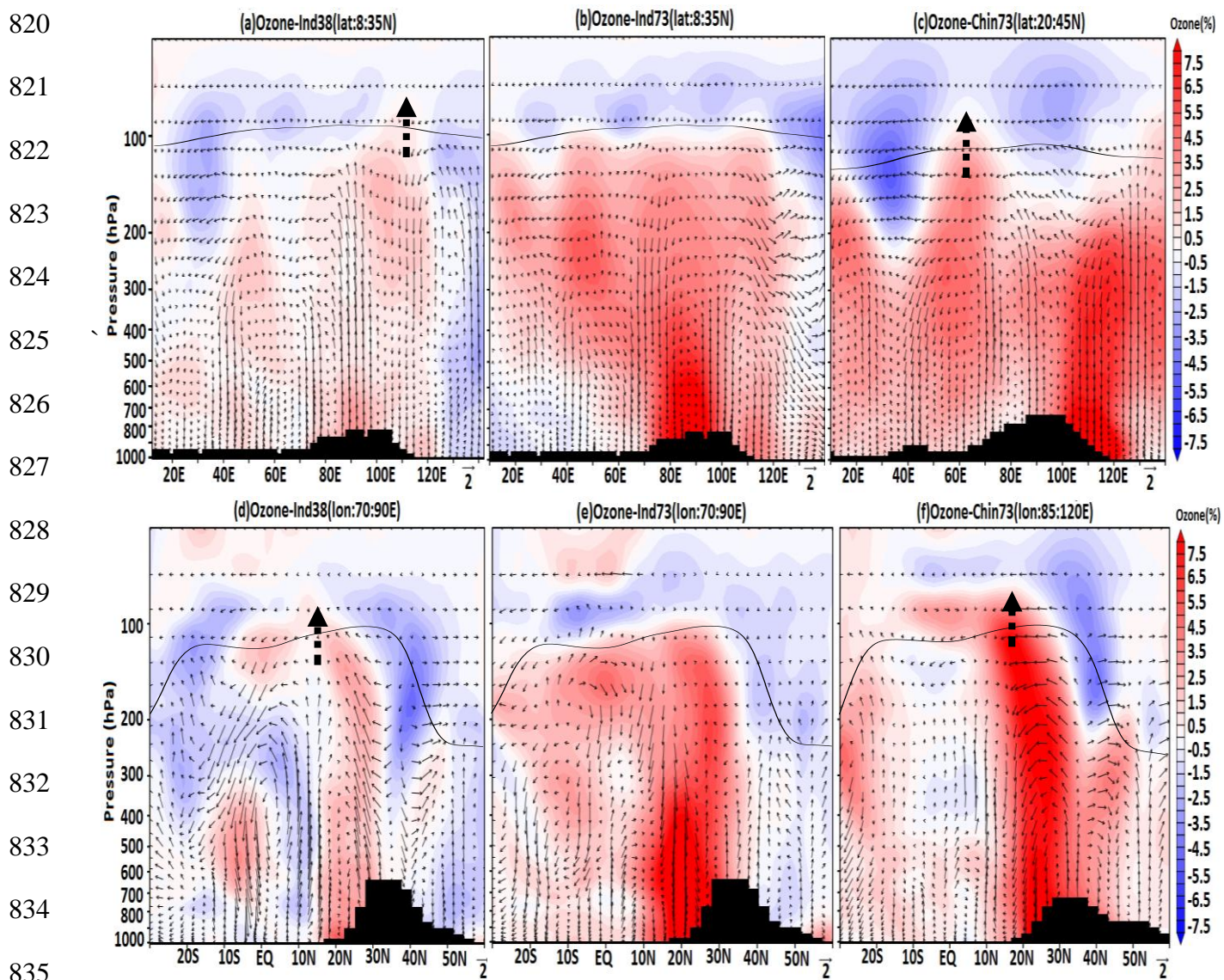
816

817

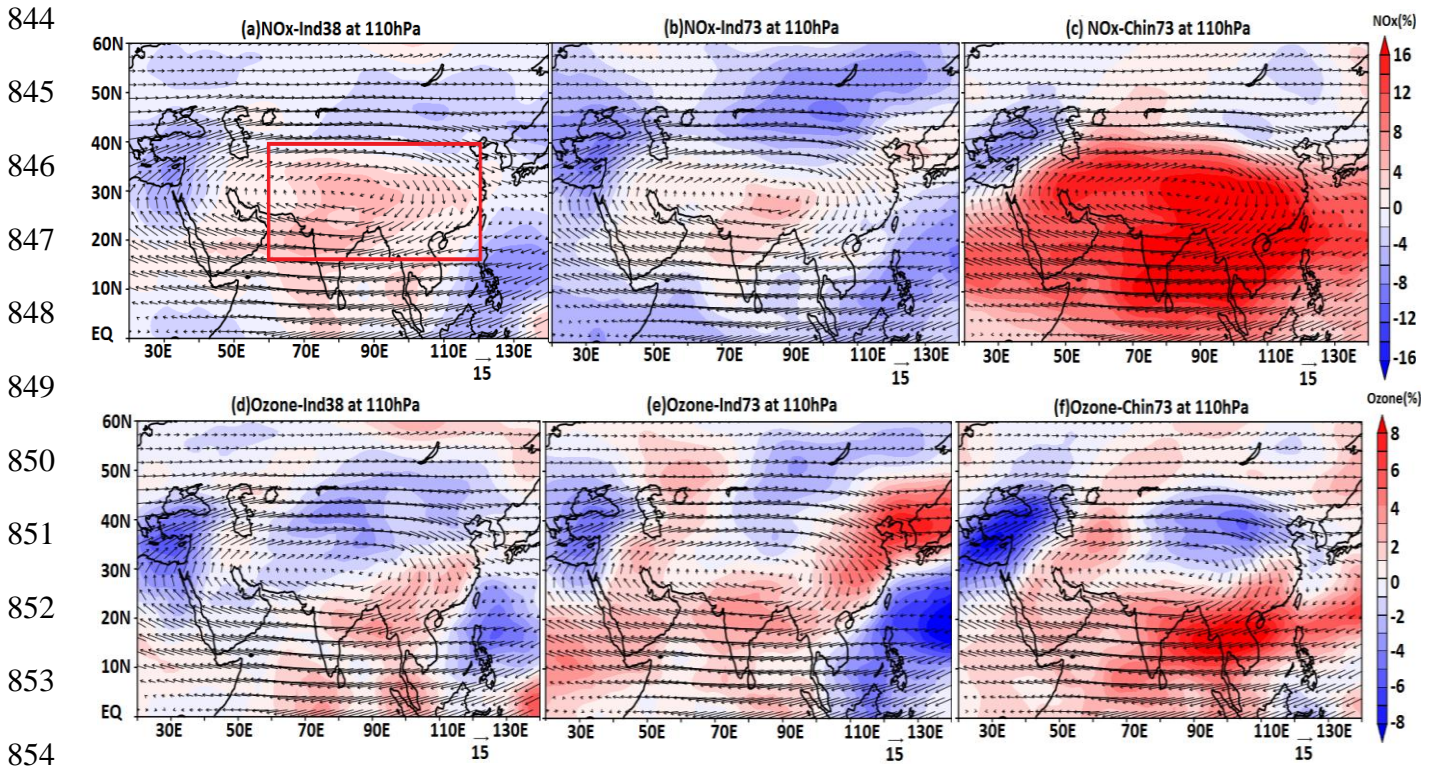
818

819

Figure 3: Longitude pressure cross-section of changes in net ozone production (ppt/day) due to enhanced NO_x with respect to the CTRL simulation, averaged for the monsoon season (June-September) obtained from (a) Ind38 (averaged over 8°N - 35°N), (b) Ind73 (averaged over 8°N - 35°N), and (c) Chin73 (over 20°N - 45°N) simulations. The black line shows the tropopause while black contours indicate 95% confidence levels.



836 Figure 4: Longitude pressure cross-section of percentage ozone anomalies averaged for the monsoon
 837 season (June-September) obtained from (a) Ind38 (averaged over 8°N-35°N), (b) Ind73 (averaged over
 838 8°N-35°N), and (c) Chin73 (averaged over 20°N-45°N) simulations. Latitude pressure cross-section of
 839 percentage ozone anomalies averaged for the monsoon season (June-September) obtained from (d)
 840 Ind38 (averaged over 70°E-90°E), (e) Ind73 (averaged over 70°E-90°E), and (f) Chin73 (averaged over
 841 85°E-120°E) simulations. Black arrows indicate wind vectors. The vertical velocity field has been
 842 scaled by 300. The **black** line represents the tropopause, and the **black dashed arrows indicate the cross**
 843 **tropopause transport.**



855 Figure 5: Latitude-longitude cross-section of percentage NO_x anomalies averaged for the monsoon
 856 season (June-September) at 110 hPa obtained from (a) Ind38, (b) Ind73, and (c) Chin73 simulations.
 857 Panels (d-f) show the same but for percentage ozone anomalies at 110 hPa for the (d) Ind38, (e) Ind73,
 858 and (f) Chin73 simulations. Black arrows indicate horizontal winds at 110 hPa. **The red box in panel (a)**
 859 **indicates the ASM anticyclone region used to compute the associated radiative forcing regional**
 860 **average.**

861

862

863

864

865

866

867

868

869

870

871

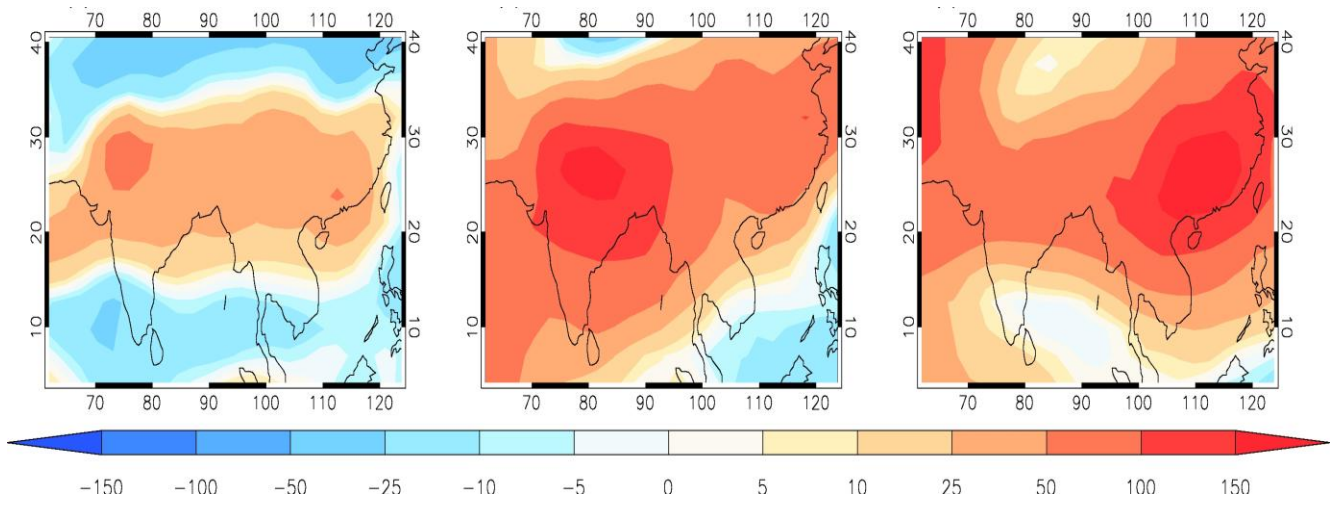


Figure 6: Latitude-longitude distribution of changes in ozone radiative forcing (in mW m^{-2}) for the (a)

Ind38, (b) Ind73, and (c) Chin73 perturbed simulations, compared to the CTRL simulation.

872

873

874

875

876

877

878

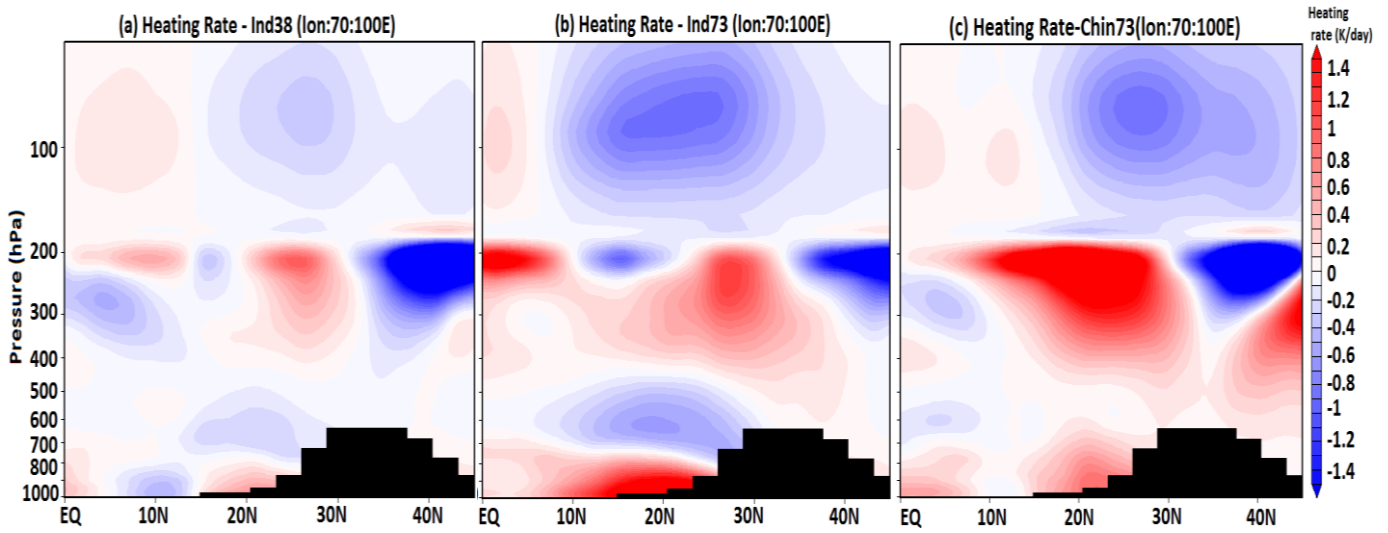
879

880

881

882

883 Figure 7: Latitude- pressure distribution of ozone heating rate changes (in K/day) for the (a) Ind38
884 (averaged over 70°-100°E), (b) Ind73 (averaged 70°-100°E), and (c) Chin73 (averaged over 90° -100°
885 E) perturbed simulations, compared to the CTRL simulation.



886

887

888

889

890

891

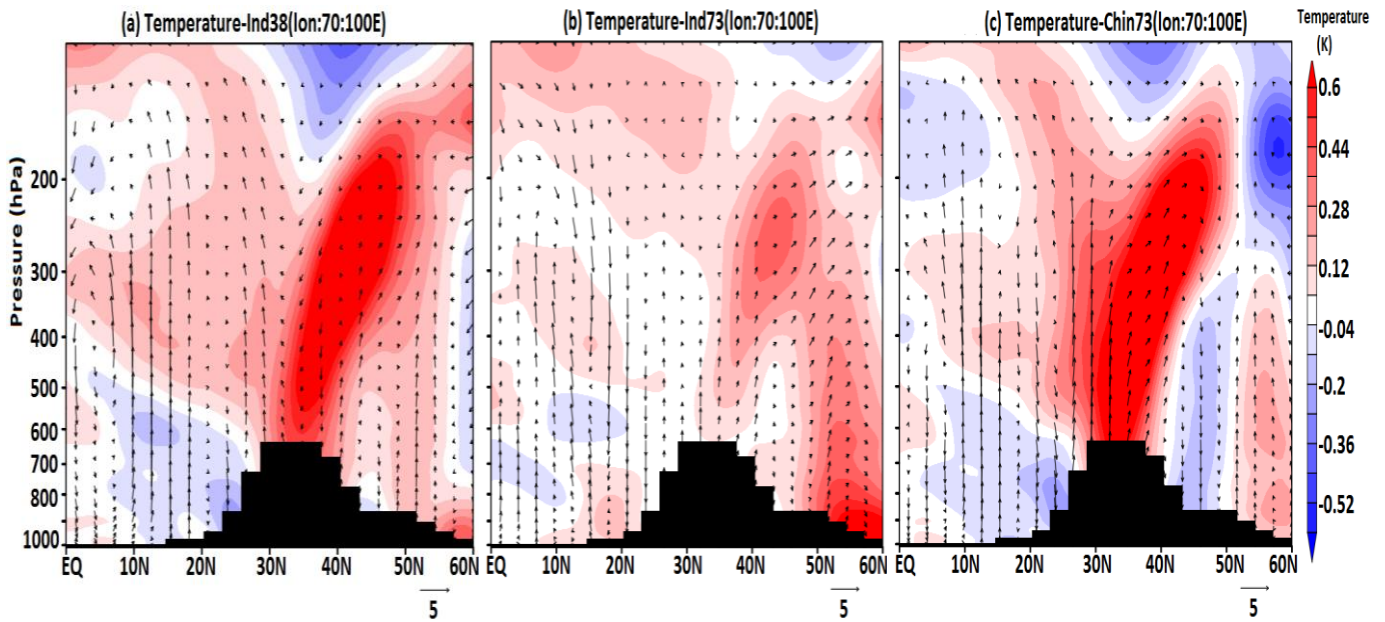
892

893

894

895

896



897

898

899

900

901

902

903

904

905

906

907

908

909

Figure 8: Latitude pressure cross-section of temperature anomalies (K) averaged for the monsoon season (June-September) and over 70°E-100°E obtained from (a) Ind38-CTRL, (b) Ind73-CTRL, and (c) Chin73-CTRL simulations. Black arrows indicate wind vectors (the vertical velocity field has been scaled by 300).

910

911

912

913

914

915

916

917

918

919

920

921

922

923

924

925

926

927

928

929

930

931

932

933

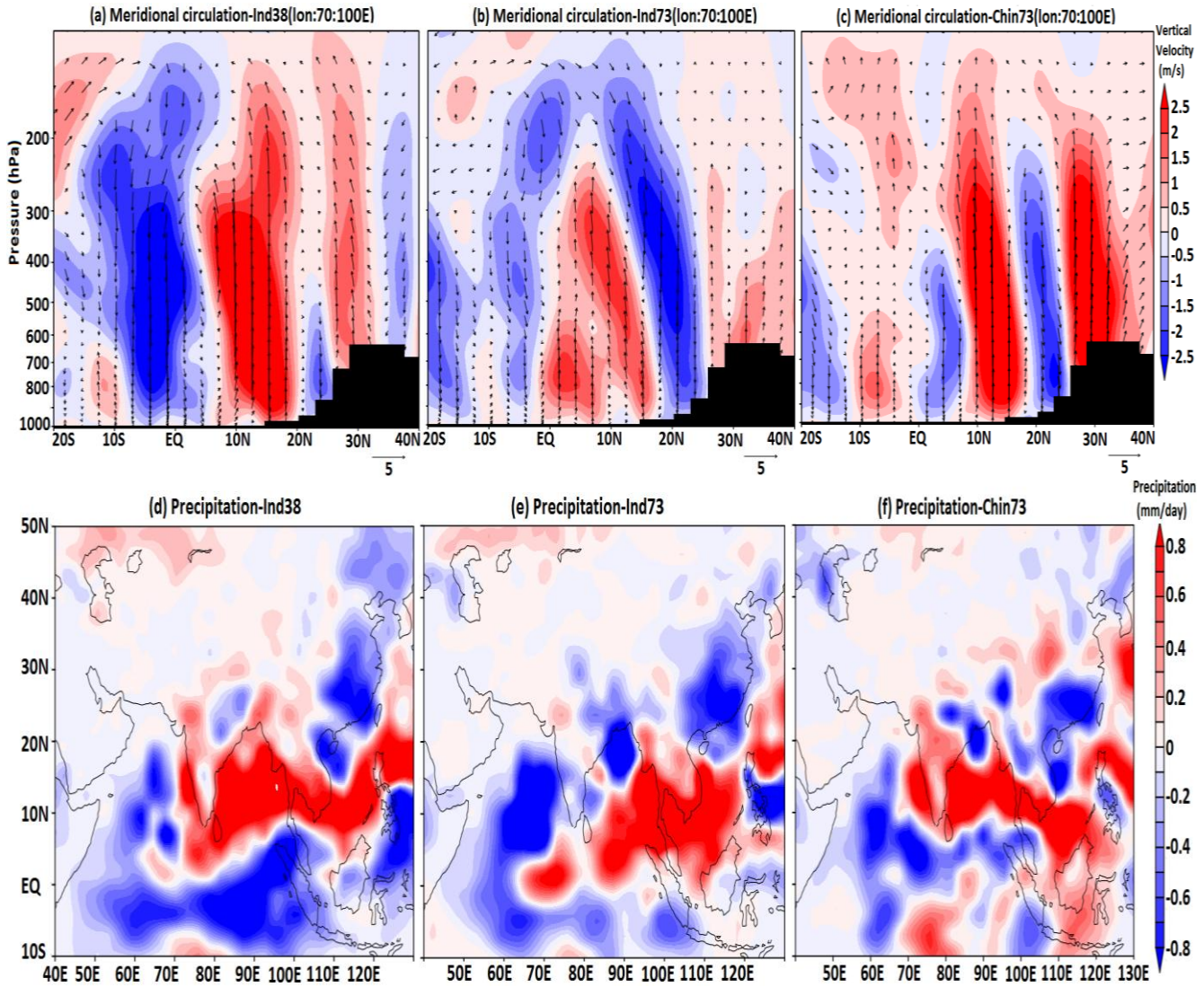


Figure 9: **Difference** in the meridional circulation due to enhanced NO_x emissions averaged for the monsoon season (June-September) and over 70°E - 110°E for (a) Ind38-CTRL (b) Ind73-CTRL (c) Chin73-CTRL simulations. Shaded contours indicate the anomalies in vertical velocity (m/s). **The vertical velocity field has been scaled by 300.** Precipitation anomalies (mm/day) averaged for the monsoon season (June-September) obtained from (d) India38-CTRL (e) Ind73-CTRL, **and** (f) Chin73-CTRL simulations.

934

935

Supplementary Figures

936

937

938

939

940

941

942

943

944

945

946

947

948

949

950

951

952

953

954

955

956

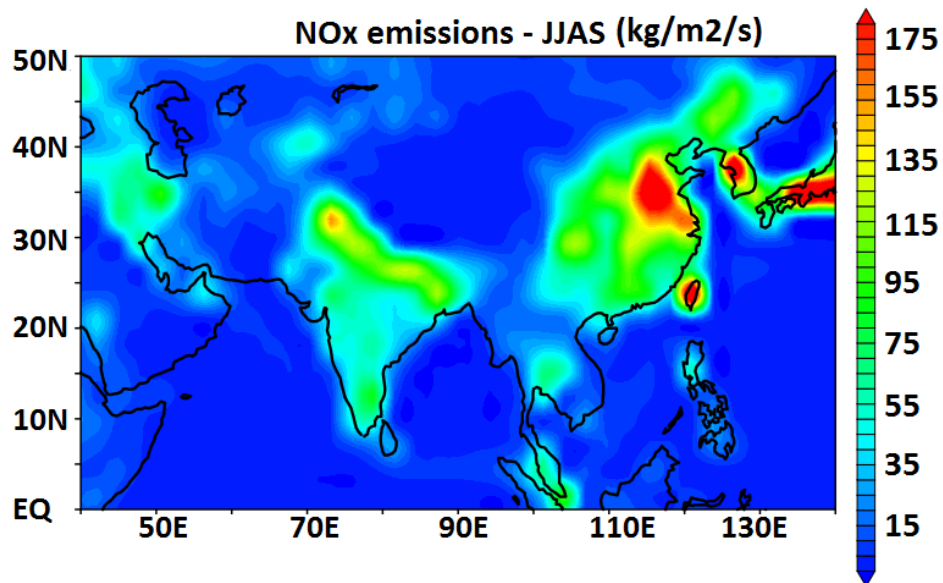


Figure S1: Distribution of NO_x emission mass flux ($\text{kg m}^{-2} \text{s}^{-1}$) from RETRO project data set for the year 2000, averaged for the monsoon season (June-September).

957
958
959
960
961
962
963
964
965
966
967
968

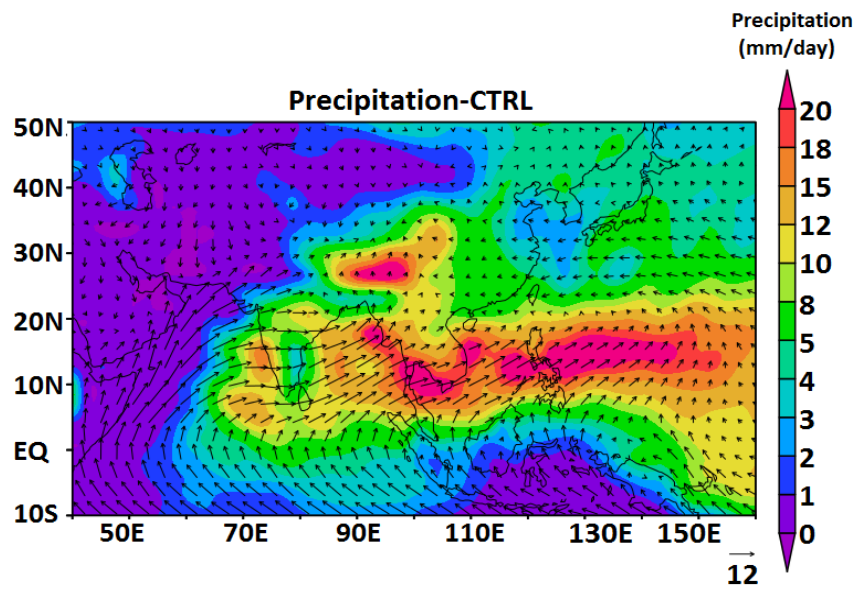


Figure S2: Distribution of seasonal (June-September) mean precipitation (mm/day) as obtained from CTRL simulation. Black arrows indicate winds (m/s).

969

970

971

972

973

974

975

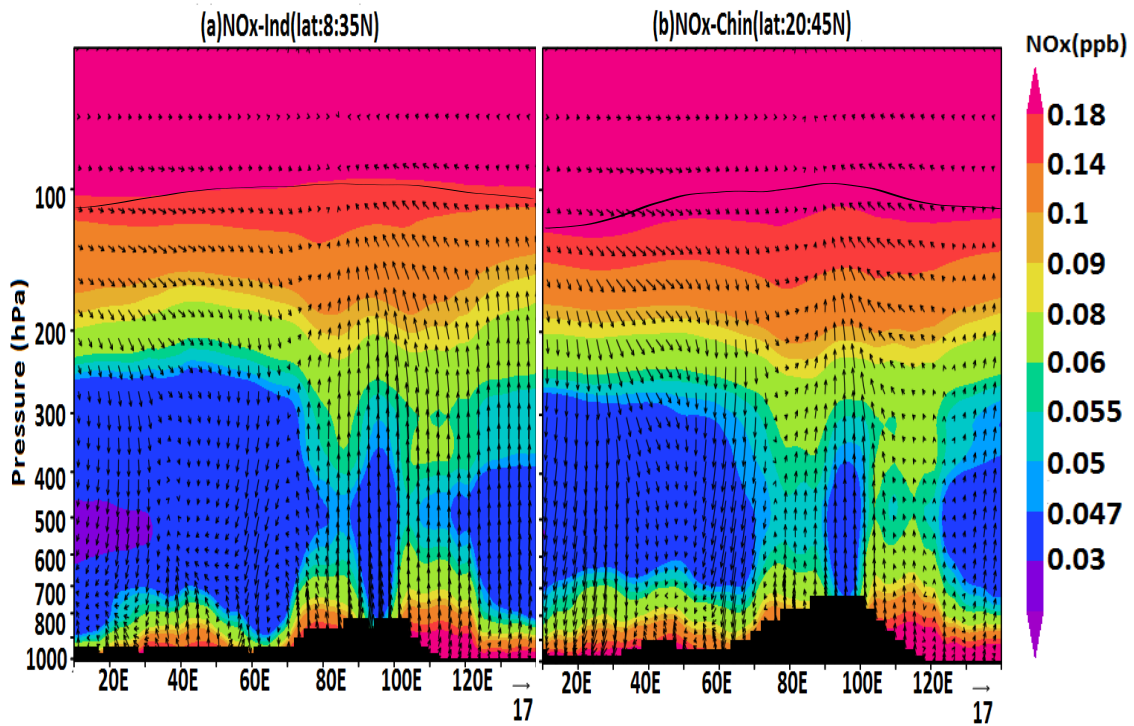
976

977

978

979

980



981 Figure S3: Vertical distribution of NO_x (ppb) averaged for the monsoon season (June-September) over

982 (a) India (8°-35°N) and (b) China (20°-45°N) as obtained from CTRL simulations. Black arrows

983 indicate winds (m/s) (the vertical component has been scaled by 300) and the black line represents the

984 tropopause.

985

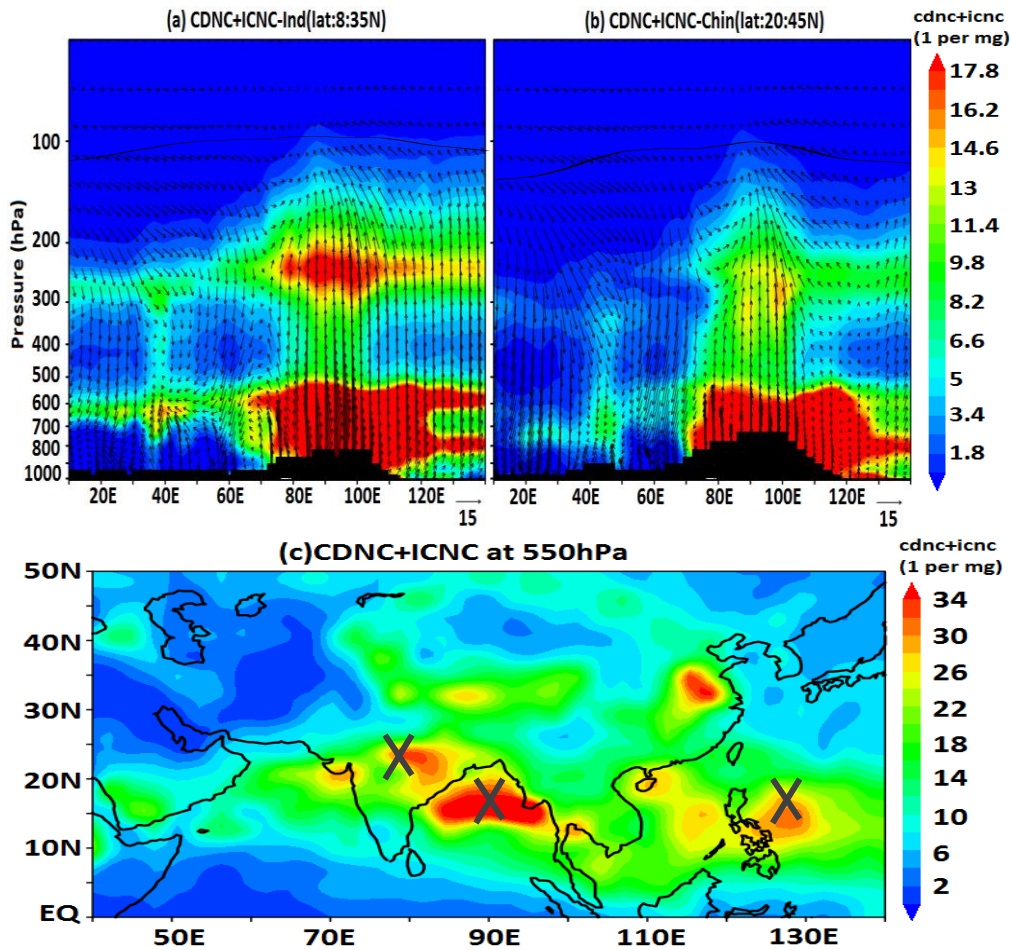
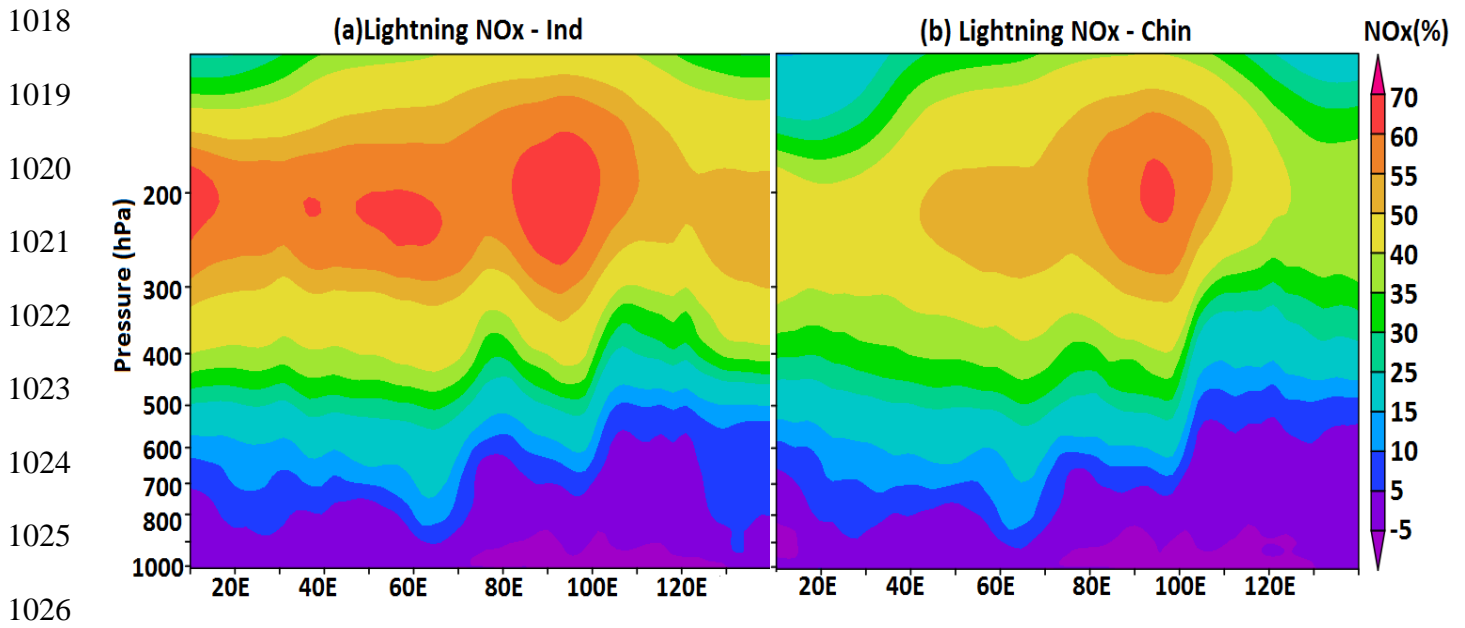


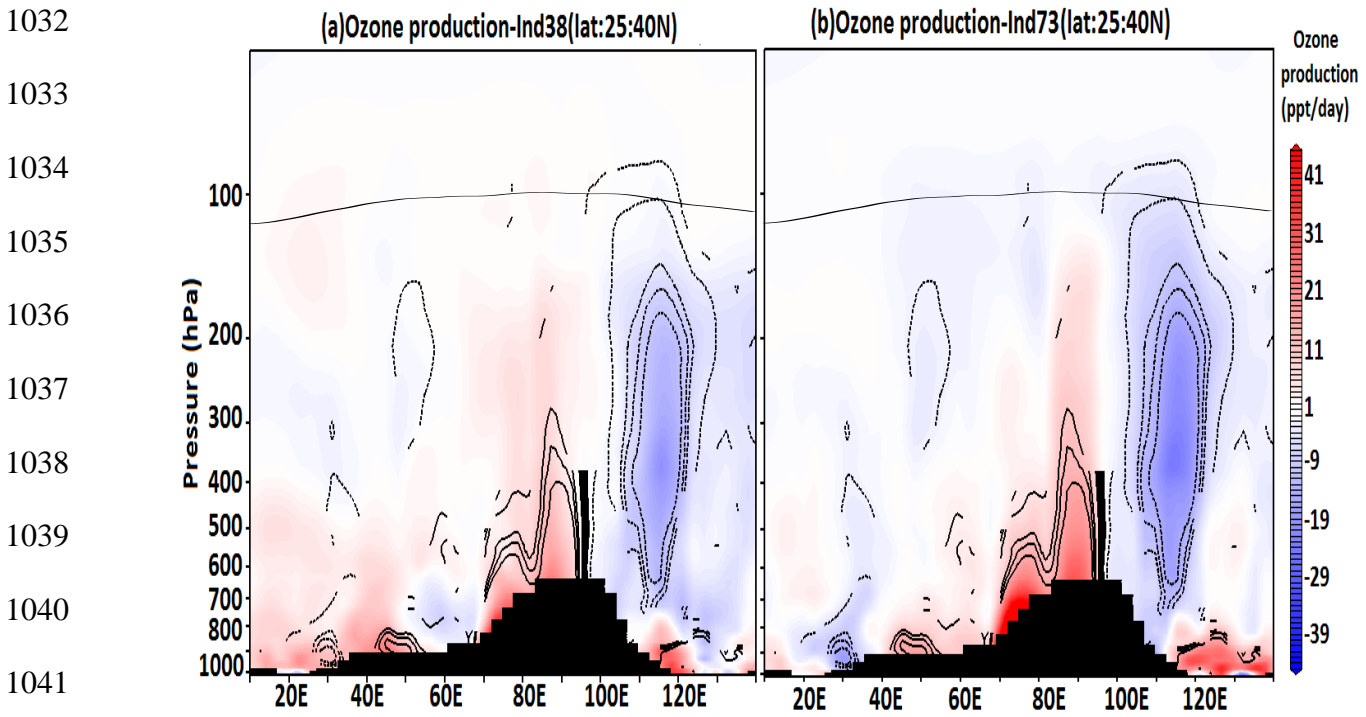
Figure S4: Distribution of combined cloud droplet (CDNC) and ice crystal (ICNC) number concentrations (in mg^{-1}) averaged for the monsoon season (June-September) over (a) India (8° - 35°N) and (b) China (20° - 45°N) as simulated in the CTRL simulation. Black arrows indicate winds (m/s) (the vertical component has been scaled by 300), and the black line represents the tropopause. (c) Distribution of seasonal (June-September) mean combined CDNC+ICNC (in mg^{-1}) at 550 hPa as simulated in the CTRL simulation. The regions of Bay of Bengal, South China Sea and southern slopes of Himalayas are indicated with a cross symbol.



1027 Figure S5: Vertical distribution of percentage NO_x anomalies produced from lightning, averaged for the
 1028 monsoon season (June-September) over (a) India (8°-35°N) and (b) China (20°-45°N), simulated by
 1029 comparing the CTRL-Lightning-on and the CTRL-Lightning-off experiments.

1030

1031



1042

1043 Figure S6: Longitude pressure cross-section of changes in net ozone production (ppt/day) due to
 1044 enhanced NO_x with respect to the CTRL simulation, averaged for the monsoon season (June-
 1045 September) and over the Indo-Gangatic plain-Tibetan Plateau region (25°N - 40°N) for (a) Ind38 (b)
 1046 Ind73. The black line shows the tropopause while black contours indicate 95% confidence levels.

1047

1048